Matter

CellPress

Review

Open the door to the atomic world by single-molecule atomic force microscopy

Siyuan Fang[1] and Yun Hang Hu[1,*]

SUMMARY

Single-molecule atomic force microscopy (sm-AFM) is a state-of-the-art AFM involving single-molecule tip functionalization, characterization, and manipulation. The pioneering work of tip functionalization with a CO molecule in 2009 realized an unprecedented atomic resolution, allowing the elucidation of chemical structures in real space with a superior single-molecule sensitivity. Furthermore, as an atomically precise manipulation tool, sm-AFM realizes both lateral and vertical movements of single molecules and even single atoms. Meanwhile, as a compatible on-surface reactor, sm-AFM enables the creation and *in situ* imaging of novel molecules and radicals that has never been achieved via conventional approaches. Endowed with these extraordinary capabilities, sm-AFM takes us into the atomic world. In this review, we reveal the principle and working condition of sm-AFM, provide up-to-date understanding on characterization, atomic manipulation, and on-surface reactions using sm-AFM, evaluate current methods for image simulation, and further outline the challenges and future perspectives for the development of sm-AFM.

INTRODUCTION

Atomic force microscopy (AFM), which works based on the interactions between the tip and the molecule-substrate system, was invented by Binnig, Quate, and Gerber in 1986.[1] Despite the high z-axial resolution, the resolution for the x axis and y axis remained low until the exploitation of the tip functionalization with a CO molecule at ~5 K by Gross and coworkers in 2009.[2] Owing to the atomically well-defined tip apex and its mechanical flexibility, unprecedented atomic resolution was achieved, allowing a clear visualization of the chemical structure of individual pentacene molecules. This demonstrates the capability of AFM as a direct characterization technique to reveal the molecular structure in real space with a rare single-molecule sensitivity, outperforming conventional approaches by which the molecular structure can only be speculated from molecular mass, crystallinity, vibration, magnetism, etc., and only an ensemble property is provided. This breakthrough has created a new generation for AFM, single-molecule AFM (sm-AFM), which uses a single molecule for tip functionalization and/or is used for characterization and manipulation of single molecules.

Stimulated by this excellent work, a number of efforts have been made to unveil the mysterious atomic world. In 2012, it became possible to discriminate the order of intramolecular C-C bonds even with a tiny bond length difference of 0.03 Å,[3] while later, in 2013 and 2017, the real-space visualization of intermolecular hydrogen bonds and halogen bonds were realized, respectively.[4,5] In addition to widely investigated organic compounds, the internal structure and adsorption geometry of

Progress and potential

Single-molecule atomic force microscopy (sm-AFM) is a new generation of AFM using a single molecule for tip functionalization and/or being used for characterization and manipulation of single molecules. The past decade has witnessed an ongoing series of stunning breakthroughs in sm-AFM. On the one hand, molecular structure, interatomic bond, and adsorption geometry have been clearly visualized in real space with a unique single-molecule sensitivity. On the other hand, atomically precise manipulation by the tip has revealed numerous intriguing physical phenomena and induced a plethora of on-surface chemical reactions. These extraordinary abilities open the door to the atomic world. This review provides an up-to-date overview on characterization, manipulation, and on-surface reactions by sm-AFM and further outlines future directions on improvement of equipment, elucidation of molecular structure, and mechanism investigation.

metal single atoms and clusters have been revealed as well.[6] More importantly, since the pioneering work in 2013, sm-AFM has enabled the elucidation of the pathway of single-molecule chemical reactions by capturing images of the elusive intermediate species.[7] This method also allows the identification of the physical transition mechanism, as demonstrated in a recent report on 2D hexagonal ice growth.[8] As a result, a deep mechanistic understanding down to the atomic level has been developed.

Furthermore, sm-AFM provides the possibility to manipulate single molecules and even single atoms, such as pulling, pushing, lifting, and charging, revealing a number of intriguing physical phenomena.[9–15] Among these approaches, lifting has received the most attention over the last 5 years, ranging from conductance measurement[16] and friction evaluation[9] to fabrication of single-electron field emitters[10] and electrostatic catalysis.[11] Moreover, very recently, an atomic-scale origami was achieved by precisely folding and unfolding nanographene with a controllable twisting angle.[17] Another important aspect of single-molecule manipulation is to induce on-surface reactions to create novel molecules and radicals by bond dissociation and skeleton rearrangement.[18–22] Also, insights into on-surface reactions are acquired, enabling accurate real-space characterization of single-molecule switches.[13] In comparison with single-molecule manipulation, thermal annealing is advantageous for synthesizing larger defect-free molecules with repeating units, such as polymers[23,24] and graphene nanoribbons.[25–28]

As the most promising equipment, sm-AFM has undergone rapid development in atomically precise characterization, manipulation, and on-surface reactions in the last few years. Despite the publication of some well-written review articles,[29–31] they mainly focus on a certain aspect of sm-AFM application, but a comprehensive overview of this advanced technique is still lacking. Moreover, a series of breakthroughs have been made since 2017, such as the elucidation of molecular structures with charge-state control,[14] the detection of spin distribution,[32,33] and the on-surface synthesis of the first pure carbon ring,[18] which were not included in previous reviews. Here, with an emphasis on the progress since 2017, we (1) reveal the origin of atomic contrast and the aspects determining the atomic resolution, (2) thoroughly discuss the application of sm-AFM as a characterization tool to elucidate the molecular structure, interatomic bond, and adsorption geometry for both pure chemicals and complex mixtures, (3) provide state-of-the-art understanding and technique of atomic manipulation from both physical and chemical perspectives, (4) elucidate the main types of thermally induced on-surface reactions, (5) evaluate current methods for image simulation, and finally (6) outline the challenges and future research directions for the application and development of sm-AFM.

HOW TO ACHIEVE ATOMIC RESOLUTION?

In general, atomic resolution is achieved by sm-AFM with a CO-functionalized tip, using frequency modulation at a constant height, in ultrahigh vacuum, at ultralow temperature, and using a qPlus sensor (as shown in Figure 1). In this section, the origin of the atomic contrast in sm-AFM images is revealed first, followed by a discussion on the factors determining the atomic resolution, and then the general operational procedure for atomic imaging and the concerns for data extrapolation are presented.

Origin of atomic contrast

The atomic contrast originates from the atomic forces as well as the mechanical response of the atoms to these forces.[34] Pauli repulsion, caused by the overlap

[1]Department of Materials Science and Engineering, Michigan Technological University, 1400 Townsend Drive, Houghton, MI 49931-1295, USA

*Correspondence: yunhangh@mtu.edu

https://doi.org/10.1016/j.matt.2021.01.013

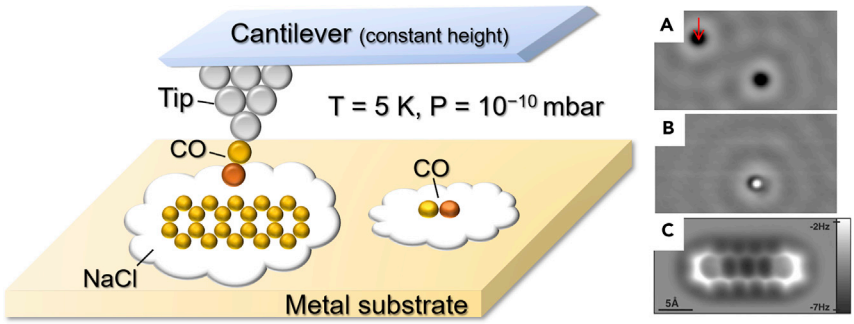

Figure 1. Schematic sm-AFM imaging

(A) Image before picking up a CO molecule (as indicated by the red arrow).

(B) Image after picking up a CO molecule.

(C) Constant-height sm-AFM image of pentacene obtained with a CO-functionalized tip. Reprinted with permission from Gross et al.[2] Copyright 2009, The American Association for the Advancement of Science.

between the electron densities of the imaged molecule and the tip apex, is the main contributor to the atomic contrast. This results in a positive shift of the oscillation frequency of the cantilever, thus showing as bright features in the constant-height sm-AFM images (see Figure 1C for an example).[2] Typically, the brighter the region is, the higher electron density it possesses, by which the molecule structure (i.e., atom position and bonding) can be clearly identified. In contrast, the attractive interactions, which include van der Waals force and electrostatic force, cause negative frequency shifts. The local attractive interactions induce the formation of a dark halo surrounding the bright molecule, while the non-site uniform interactions between the tip and the substrate provide a gray background in the constant-height sm-AFM images.[34]

Frequency-modulated mode at constant height

sm-AFM using frequency modulation at a constant height is preferred for atomic imaging. In this mode, the tip held by the cantilever oscillates at resonance in a constant amplitude as controlled by two feedback circuits (one for resonance frequency and the other for constant amplitude).[35] The tip-sample interaction results in a frequency shift, which can be measured by the equipment. To achieve atomic resolution, the oscillation amplitude must be down to ~1 Å to ensure the sensitivity to short-range forces, while the tip height is generally set as ~4 Å above the sample.[31] Within a small amplitude, the frequency shift is in direct proportion to the gradient of the force between the tip and the sample.[34] Such a non-contact frequency-modulated mode at a constant height is advantageous due to the following aspects. On the one hand, destruction of the tip and the sample can be avoided. On the other hand, compared with the constant-frequency-shift mode, operational stability and signal-to-noise ratio are improved because there is no need for feedback circuit to control the tip height.[2,35] However, it should be mentioned that the constant-height operation may fail on non-planar molecules due to complex image contrast and undesirable contact.

Ultrahigh vacuum

Ultrahigh vacuum, typically below 10^{-10} mbar, ensures the formation of a clean atomically flat substrate, which not only avoids contamination of the tip but also enhances the resolution of the target molecule.[2,18] Furthermore, when inducing an on-surface reaction via atomic manipulation, ultrahigh vacuum can effectively exclude the side reactions with the substances in the environment and, meanwhile,

offer an accurate temperature control, which is particularly important for temperature-sensitive surface reconstruction.[30] However, the use of the ultrahigh vacuum limits the introduction and further investigation of volatile species.

Low temperature

A temperature as low as 5 K, achieved by using a liquid helium bath cryostat, is generally required. First, a low temperature can freeze and thus isolate and stabilize the molecules, including the one to be imaged and the one for tip functionalization. Second, the vacuum is improved at low temperature, ensuring the cleanliness of the sample. Third, the quality factor of the sensor as well as the mechanical stability are enhanced.[31] Due to the above aspects, ensuring a low temperature is the key to atomic imaging.

Tip

The exploitation of an inert atomically sharp tip is of vital importance to achieve atomic resolution. Cu and PtIr are the most widely used raw materials for the sm-AFM tip.[2,18] Due to the high reactivity of metals, chemical bonding can be easily formed between the metal tip and the molecule, which will result in the lateral or vertical manipulation of the molecule.[2] This is desirable for inducing on-surface reactions but adverse to atomic imaging. To achieve atomic imaging, the metal tip is functionalized by picking up an inert atom or molecule, which not only prevents unintentional movement of the target molecule but also enhances the resolution because the tip radius is lowered down to the atomic scale (equal to the radius of the terminating atom).[2,3]

So far, CO,[2] NO,[36] CuO,[37] Si,[38] halogens (Cl, Br, and I),[2,36] and noble gases (Xe and Kr),[36,39] have been explored for tip functionalization. Compared with single atoms, diatomic molecules are advantageous to achieve high resolution due to their easy tilting at the tip apex, which results in very sharp features in the sm-AFM images.[3] Furthermore, the type of the second-frontmost atom and the stability of the functionalized molecule can directly influence the atomic contrast.[36] Combining all of these aspects, CO has been widely utilized to acquire atomic-resolution sm-AFM images.

The images before and after picking up one CO molecule are shown in Figures 1A and 1B, respectively, where the appearance of the other CO molecule changed from a depression to a protrusion. The CO molecule adsorbs with its carbon atom connected with the metal tip, with certain mechanical flexibility.[3] The tilting of CO induced by Pauli repulsion and van der Waals force causes apparent distortions and thereby the sharp bond features. This amplifies the difference in bond lengths by nearly one order of magnitude, rendering it possible to discriminate the bonds with a length difference down to 0.03 Å.[3] However, CO tilting might also result in artifacts appearing as bonds,[40] which actually represent the ridge of the potential energy landscape caused by neighboring atoms.[34] Fortunately, the approach to correct the distortion effects has been developed by connecting the lateral distortion and the force.[41]

qPlus sensor

The force sensor is the core of sm-AFM. The qPlus sensor, which is built from quartz, is capable of self-sensing due to the piezoelectricity effect.[42] The stable frequency (~30 kHz), small oscillation amplitude (<1 Å), and stiffness of quartz contribute to the enhancement in the signal-to-noise ratio. With such an accurate sensor, the conservative and dissipative interactions can be separated, with the

former inducing the frequency shift and the latter altering the feedback circuit to maintain a constant oscillation amplitude.[43] Also, the simultaneous scanning tunneling microscopy (STM) measurement is realized without deterioration of the performance.

General operational procedure

The general operational procedure is as following. First, clean the substrate, i.e., the single metal crystal with a low index plane, such as Cu(111), Au(111), and Ag(111), by repeated sputtering and annealing cycles. Second, shape the tip by *in situ* indentations into the metal substrate. Third, transfer NaCl onto the metal substrate (at ~270 K) via sublimation, forming inert NaCl islands. Fourth, introduce CO into the chamber (2×10^{-8} mbar) to allow its adsorption on the substrate (at 10 K). Fifth, deposit the sample (with a molecular mass of 100–10,000 Da) to the substrate (at 10 K) via evaporation or sublimation from a flash-annealed Si wafer. Sixth, use the tip to pick up one CO molecule (at 5 K) for tip functionalization. Seventh, image the sample in the constant-height mode (at 5 K). The third, fourth, and sixth steps may be skipped or modulated in some cases.

Data extrapolation

Since sm-AFM is conducted under an extreme condition and the sample is adsorbed on a certain surface, any extrapolation of acquired results should be treated cautiously. First, although the use of ultralow temperature shows little influence on the chemical bonding thus being able to provide a reliable chemical structure, it can affect the physical configurations and properties (electrical conductivity, magnetism, etc.) of the sample.[44–46] For example, the magnetism would be enhanced at ultralow temperature due to the suppressed para-magnetism resulting from the reduction of the kinetic energy. Second, because the sample is adsorbed on a substrate, its structure and properties are directly affected by the substrate, making it different from free molecules and molecules in solution. Third, the main role of ultrahigh vacuum is to ensure the cleanliness of the system while it can also quickly remove the volatile species and gas molecules. The above three aspects must be taken into consideration before data extrapolation.

SEEING SINGLE MOLECULES

The most straightforward application of sm-AFM is to image the molecules, by which the molecular structure, composing element, interatomic bond, and adsorption geometry can be directly seen. Besides, sm-AFM is capable of visualizing multiple intermediates and products in chemical reactions as well as naturally occurring mixtures. Extension of sm-AFM techniques further realizes the detection of the electronic and magnetic properties. These aspects will be amply discussed in this section with an emphasis on recent progresses.

Molecular structure

sm-AFM is a powerful tool enabling us to directly see the structure of the molecule, outperforming conventional approaches by which we could just speculate the structure. In their pioneering work, of 2009, Gross et al.[2] demonstrated imaging of pentacene with an unprecedented atomic resolution by functionalizing the tip with a CO molecule, where the five hexagonal carbon rings and even the C-H bonds of pentacene were clearly seen (Figure 1C). Motivated by this great breakthrough, a number of efforts have been made to image a wide range of molecules, including hydrocarbons,[7,47–49] nanographene,[25,26,50] graphdiyne,[51] polyyne,[19,52] cyclocarbon,[18,53] C60,[54] borophene,[55,56] h-BN,[57] WS_2,[58] and metal single atoms and clusters.[6]

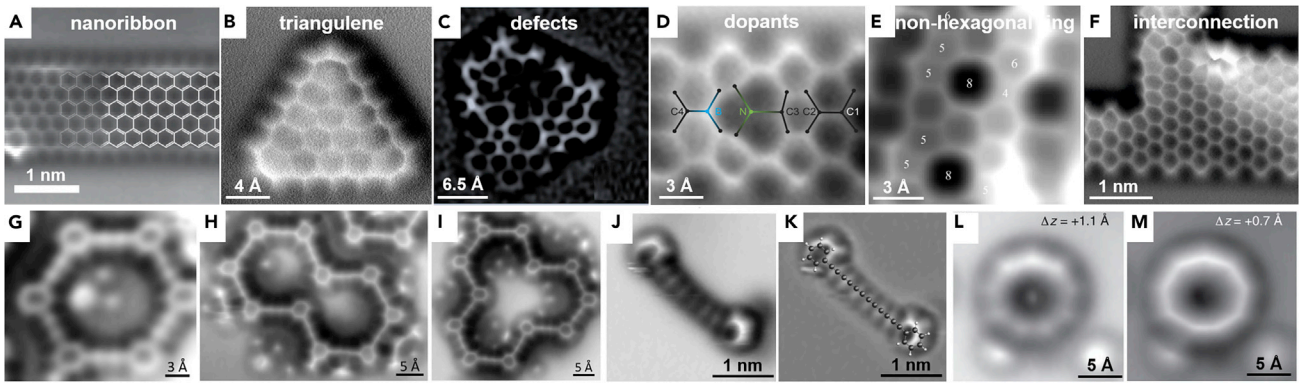

Figure 2. sm-AFM images of carbon allotropes

(A) Zigzag graphene nanoribbon. Reprinted with permission from Ruffieux et al.[26] Copyright 2016, Springer Nature.

(B) π-Extended [5]triangulene. Reprinted with permission from Su et al.[50] Copyright 2019, The American Association for the Advancement of Science.

(C) Defects in trigonal nanographene. Reprinted with permission from Zuzak et al.[59] Copyright 2019, The Royal Society of Chemistry.

(D) B- and N-doped graphene. Reprinted with permission from Kawai et al.[62] Copyright 2018, The American Association for the Advancement of Science.

(E) Graphene nanoribbon with non-hexagonal rings. Reprinted with permission from Liu et al.[65] Copyright 2018, American Chemical Society.

(F) Junction between graphene nanoribbons. Reprinted with permission from Dienel et al.[66] Copyright 2015, American Chemical Society.

(G–I) (G) 6-membered graphdiyne macrocycle, (H) 10-membered graphdiyne macrocycle, and (I) 12-membered graphdiyne macrocycle. Reprinted with permission from Liu et al.[51] Copyright 2018, American Chemical Society.

(J and K) (J) Hexayne (sp-hybridized carbon chain) and (K) its Laplace-filtered image with ball-and-stick model. Reprinted with permission from Pavliček et al.[19] Copyright 2018, Springer Nature.

(L and M) Cyclo[18]carbon (sp-hybridized carbon ring) imaged at (L) large and (M) small tip offsets. Reprinted with permission from Kaiser et al.[18] Copyright 2019, The American Association for the Advancement of Science.

Owing to the stabilization effect of low temperature and the atomic resolution of sm-AFM, a series of nanographene materials have been successfully imaged, such as graphene nanoribbon (Figure 2A) and triangulene (Figure 2B).[26,50] Furthermore, sm-AFM enables the direct visualization of the specific structural features of graphene, including defects, dopants, non-hexagonal rings, and interconnections. First, defects, which are generally deduced from Raman spectra, can be directly seen in the sm-AFM images (Figure 2C).[59,60] More importantly, the observed structural distortion around the defect implies some unique chemical and physical properties (e.g., electrical conductivity and magnetism).[60,61] Second, B and N dopants in graphene and the resultant adjustment of nearby bond lengths, have been illustrated via sm-AFM (Figure 2D), attributed to the different van der Waals radii of atoms and the changing local electron density, respectively.[55,62,63] In contrast, O and S atoms can only locate at the edge of graphene due to their divalent nature.[64] Third, non-hexagonal rings, as a type of defects breaking the sublattice symmetry but still keeping the sp^2 hybridization, have also been detected in graphene (Figure 2E).[65] Here, since the carbon ring transformation is thermally sensitive, temperature-adjustable sm-AFM offers an effective approach to investigate the thermal stability and the structural transition of non-hexagonal rings in graphene.[65] Fourth, the structural mismatch at the interconnection of armchair and zigzag graphene nanoribbons (Figure 2F) has also been revealed, where the non-hexagonal carbon rings appear, which further leads to the structural non-planarity within the junction.[66]

Graphdiyne, which is composed of sp^2- and sp-hybridized carbon atoms, is even more intriguing than graphene, due to its high π content, rich pores, and diverse structures.[67] As a novel approach, a series of graphdiyne macrocycles were *in situ* synthesized by assembling and coupling reactions on Au(111) in sm-AFM (the images are shown in Figures 2G–2I).[51] More importantly, sp-hybridized carbon, which is the most mysterious member in the carbon family due to its high chemical reactivity, has

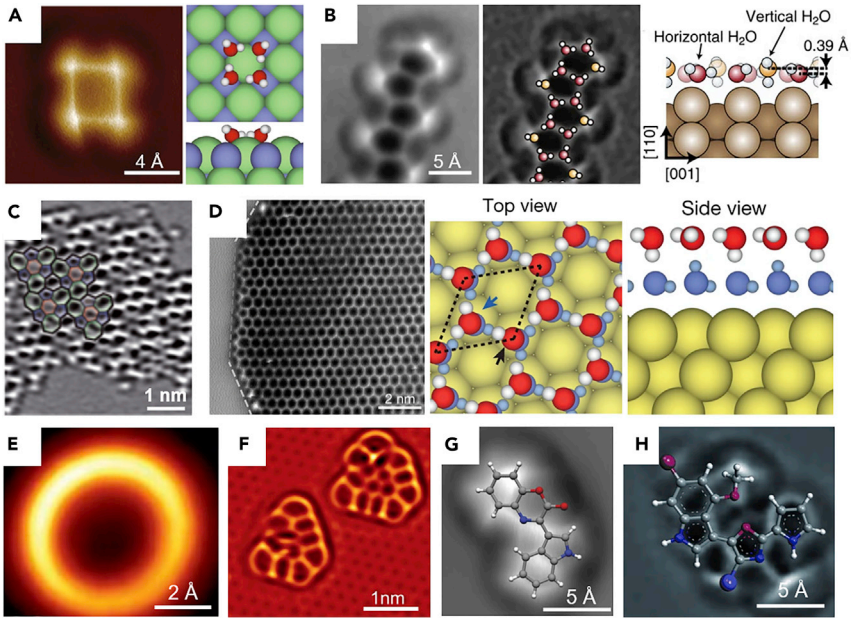

Figure 3. sm-AFM images and corresponding models of water molecule assemblies, metals, and natural compounds

(A) Cyclic water tetramer on NaCl(001) (white, H; red, O). Reprinted with permission from Peng et al.[68] Copyright 2018, Springer Nature.

(B) 1D water chain composed of pentagonal rings on Cu(110) (white, H; red and yellow, O). Reprinted with permission from Shiotari et al.[70] Copyright 2017, Springer Nature.

(C) 2D water network on Ni(111). Reprinted with permission from Shiotari et al.[69] Copyright 2019, American Physical Society.

(D) 2D water network on Au(111) (white and light blue, H; red and dark blue, O). Reprinted with permission from Ma et al.[8] Copyright 2020, Springer Nature.

(E and F) (E) Cu single atom and (F) Fe clusters. Reprinted with permission from Emmrich et al.[6] Copyright 2015, The American Association for the Advancement of Science.

(G) Cephalandole A (white, H; gray, C; blue, N; red, O). Reprinted with permission from Gross et al.[71] Copyright 2010, Springer Nature.

(H) Hydrozoan *Thuiria breitfussi* (white, H; gray, C; small blue, N; large blue, I; small purple, O; large purple, Br). Reprinted with permission from Hanssen et al.[72] Copyright 2012, Wiley-VCH Verlag GmbH & Co. KGaA, Weinheim.

been captured by sm-AFM.[18,19] Both carbon chain (Figures 2J and 2K)[19] and carbon ring (Figures 2L and 2M)[18,53] were successfully created and seen on an inert NaCl surface at 5 K, where the polyynic structure can be clearly identified based on the characteristic nodes in the triple bonds, which is further discussed in Interatomic bond.

Interestingly, similar to carbon atoms, water molecules can arrange in various manners via hydrogen bonds, as controlled by the surface type and temperature.[8,68–70] The weak high-order electrostatic interaction between the CO-functionalized tip and the strongly polar water molecules allows the atomic imaging with little disturbance.[68] Four water molecules could combine into a cyclic water tetramer on NaCl(001) at 5 K, in which each water molecule contributes one H atom to form the hydrogen bond while the other H atom points obliquely upward (Figure 3A).[68] Moreover, the 1D water chain that is composed of pentagonal rings was observed on Cu(110) at 78 K (Figure 3B).[70] In the composing pentagonal unit, one water molecule vertically bonds to Cu at the hollow site while the others lie horizontally on Cu at the top sites. With further increase of water coverage, a 2D water network can be formed, consisting of pentagonal, hexagonal, and/or heptagonal water rings.[8,69,70]

On Ni(111) at 78 K, the basic unit of the water network contains a central hexagonal ring and surrounding alternating pentagonal and heptagonal rings (Figure 3C),[69] while on Au(111) at 120 K, a 2D bilayer water network with a well-ordered hexagonal structure was demonstrated (Figure 3D).[8] In each layer, half of the water molecules lie flat while the others lie perpendicular to the substrate with the formation of in-plane hydrogen bonds. The vertically aligned O-H bonds could form hydrogen bonds across the layer. The growing mechanism of the water network is revealed in Intermediate species.

On top of the attractive carbon allotropes and fantastic water architectures, imaging an individual atom has been achieved on metals.[6] Both Cu and Fe single atoms present similar toroidal structure (Figure 3E), arising from the electrostatic attraction at the atomic center and the Pauli repulsion in the edge. Fe clusters are shown in Figure 3F, each of which contains one Fe atom on the top. The top atom shifted during imaging, shown as a streak. Moreover, similar to organic compounds, the edges of Fe clusters appear strongly distorted.

In addition to identifying the molecular structure of above-discussed elaborately synthesized substances, sm-AFM also enables the accurate recognition of natural compounds, such as cephalandole A (Figure 3G)[71] and hydrozoan *Thuiria breitfussi* (Figure 3H).[72] For these unknown substances, sm-AFM not only allows the characterization with a very small amount of sample, but also, more importantly, directly determines the connecting positions of both carbon skeleton and substituent groups.

Composing element

Since the constant-height mode is generally used, the interaction between the tip and the atom is directly affected by the van der Waals radius of the atom. Namely, a smaller atomic radius will lead to a larger tip-atom distance, then a weaker interaction, and thereby a darker feature in sm-AFM images.[62] For example, the reported van der Waals radii of B, C, and N are 192, 170, and 155 pm, respectively,[73] thus the N atom is darker and the B atom seems brighter than C atoms in B- and/or N-doped graphene.[55,62,63] Such an atomic contrast has been also demonstrated on h-BN.[74] Here, choosing an appropriate tip height is of vital importance.

In addition to the van der Waals radii, the effects of the modulated local charge density, bonding geometry, and substrate interactions also should be carefully considered.[62,75] The combination of the local contact potential difference detected by Kelvin probe force microscopy (KPFM) (which is further discussed in Electronic properties) and the result of DFT calculations assists with element discrimination.[74] Despite the fact that B, N, O, and S have been discerned from the dominant C atoms, more efforts are still expected to further extend the element scope and enhance the contrast between different elements.

Interatomic bond

There are two types of bonds, intramolecular and intermolecular bonds, both of which have been visualized by high-resolution sm-AFM. Typically, as revealed in How to achieve atomic resolution?, a greater electron density of a bond results in a stronger Pauli repulsion, which enhances the brightness of this bond, while the tilting of the CO molecule adsorbed on the tip further amplifies the difference of apparent bond lengths.[3] In 2012, the discrimination of the order of intramolecular C-C bonds was first achieved, allowing the identification of the length difference down to 0.03 Å.[3] In the meantime, the angular symmetry of chemical bonds was revealed by connecting the force and potential energy with the angle.[76]

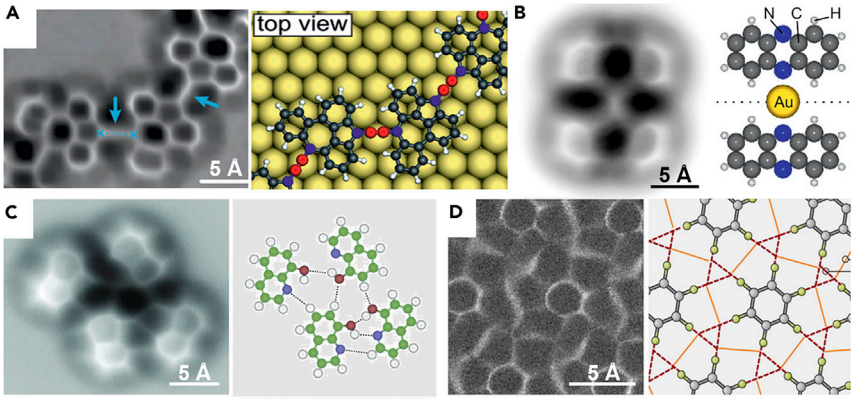

Figure 4. sm-AFM images and corresponding models illustrating the intramolecular and intermolecular bonds

(A) Cumulene-containing polymer (white, H; others, C). Reprinted with permission from Urgel et al.[78] Copyright 2020, Wiley-VCH Verlag GmbH & Co. KGaA.

(B) Phenazine-Au-phenazine complex (white, H; gray, C; blue, N; yellow, Au). Reprinted with permission from Albrecht et al.[83] Copyright 2013, American Chemical Society.

(C) 8-Hydroxyquinoline assembled cluster (white, H; green, C; blue, N; brown, O). Reprinted with permission from Zhang et al.[4] Copyright 2013, The American Association for the Advancement of Science.

(D) C_6F_6 assembled network (gray, C; yellow, F). Reprinted with permission from Han et al.[5] Copyright 2017, The American Association for the Advancement of Science.

The covalent bond is the most important intramolecular bond. Most impressively, in 2019, the bond length alternation of the first sp-hybridized carbon ring, cyclo[18]carbon, was revealed.[18] As shown in Figure 2L, at a moderate tip height, nine bright lobes were observed, which then turned into corners when the tip height was reduced (Figure 2M). The lobes and corners correspond to the triple bonds, thereby demonstrating the polyynic structure of cyclo[18]carbon, in good agreement with the image of linear carbon chain (Figure 2J).[19] This provides the first experimental evidence against the long-lasting debate about the way sp-hybridized carbon materials bond.[77] Very recently, cumulene-like bonds were generated and imaged as the bridge between tribenzoazulene molecules.[78] Namely, as shown in Figure 4A, the sharp lines linking the tribenzoazulene molecules are assigned to three consecutive C=C bonds, as supported by DFT calculations. The lengths of the middle bond and the neighboring bonds are 1.32 and 1.44 Å, respectively, indicating a stronger similarity to cumulene than polyyne. The length and order of C-C bonds have also been discriminated in aryne,[20] tetrapyrrole,[79] indeno[1,2-*b*]fluorene,[80] some polymers,[24,81,82] etc.

The coordination bond, which is a special type of covalent bond, has also been identified via sm-AFM. Coordination bonds were formed between Au and two aromatic N atoms upon applying a bias voltage, which can be clearly seen in Figure 4B, leading to the formation of a phenazine-Au-phenazine complex.[83] Here, the complex formation was reversible by simply breaking one of the Au-N bonds.

Not only the intramolecular bonds, but also the elusive intermolecular connections, have been directly identified by high-resolution sm-AFM. By quantifying the atomic force, it was found that the intermolecular contrast arises from the short-range repulsive force rather than the long-range electrostatic interactions, which enables the parallel imaging of the inter- and intramolecular features.[84] However, special attention must be paid since the intermolecular contrast might be caused by the flexibility of the tip-terminated molecule (CO in most cases).[34]

The hydrogen bond is the most representative of intermolecular bonds, and was first visualized in 2013, with its bonding site, orientation, and length revealed (Figure 4C).[4] The observed O-H···N and O-H···O hydrogen bonds are due to the covalent charge in H···N or H···O and the charge transfer from H to N and O atoms. Similar bond features are dominant in water assemblies, as discussed in Molecular structure. Interestingly, unconventional C-H···N and C-H···F hydrogen bonds have also been captured, although showing a less evident charge accumulation effect.[4,84,85] Furthermore, C-H···O=C, as a special hydrogen bond, can be formed between the hydrocarbon molecule and the tip-adsorbed CO, as a powerful tool to detect the intangible H atoms.[86]

The halogen bond is another important form of intermolecular interaction. When halogen atoms are contained in a molecule, they tend to be negatively charged due to their strong electronegativity; thus, they can attract other negatively charged species, leading to the formation of intermolecular halogen bonds.[5] As shown in Figure 4D, C_6F_6 molecules self-organize in such a manner that each F atom joins a triangular windmill structure with F atoms in two nearby C_6F_6 molecules, almost identical to the halogen-3 synthon.[5] A similar bonding arrangement was also observed in C_6Br_6 and $C_6H_3F_3$ assemblies, owing to both London dispersion and electrostatic repulsion between the terminating halogen atoms.

Some technical improvements have been made recently to realize a more accurate visualization of interatomic bonds. By using a rigid O-terminated Cu tip for imaging, the resolution for interatomic interactions can be enhanced and, more importantly, the image distortion and the systematic overestimation of the bond length are effectively avoided.[37] Furthermore, a very recent report demonstrated that, other than generally used vertical tip oscillation, lateral tip oscillation can strum the chemical bond, allowing a clear visualization and, moreover, producing measurable energy dissipation.[87]

Molecular adsorption

Molecular adsorption is the most common phenomenon in sm-AFM imaging. Namely, the target molecule to be imaged is adsorbed on the substrate while the CO molecule is adsorbed on the tip. The interaction between the tip and the molecule also can be regarded as adsorption. Here, it should be noted that the structure and properties of the molecule are affected by the substrate, and also the apparent sm-AFM images are influenced by the tip-terminating molecule, so any extrapolation must be cautiously conducted.

Metal and metal oxide substrates generally show relatively strong interactions with the molecule, influencing the adsorption strength, site, direction, etc. For metal substrates, a wider and closer d-band to the Fermi level leads to a stronger broadening of the molecular orbital and thereby a stronger adsorption.[88] While chemisorption causes molecular deformation, physisorption shows less influence on the molecular structure. Chemisorption and physisorption may co-exist in a single molecule due to the property difference of the composing atoms, which induces a non-planar configuration of the molecule; although with the same adsorption type, the adsorption height of different parts of the molecule also can be varied.[39,60,82,89,90] As shown in Figure 5A, the adsorption of the pentacene molecule on Cu(111) exhibits a valley shape with a height difference of ~0.3 Å,[39] similar to that of the anthracene unit in the oligomers.[82] Moreover, even 2D materials can be non-planar.[57] For example, the h-BN layer possesses corrugations that are 0.3–0.7 Å closer to the Cu(111) substrate.[57]

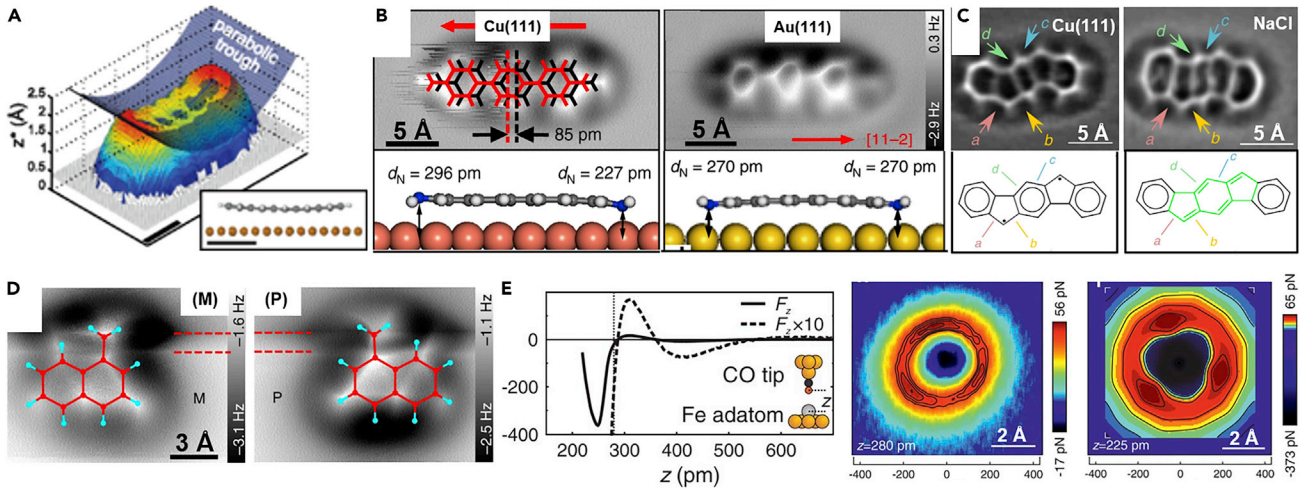

Figure 5. sm-AFM images and corresponding models of molecular adsorption

(A) Adsorption height of pentacene on Cu(111). Reprinted with permission from Schuler et al.[39] Copyright 2013, American Physical Society.

(B) Adsorption of 4,4″-diamino-*p*-terphenyl on Cu(111) and Au(111) (white, H; gray, C; blue, N). Reprinted with permission from Zhong et al.[91] Copyright 2018, Springer Nature.

(C) Adsorption of indeno[1,2-*b*]fluorene on Cu(111) and bilayer NaCl-covered Cu(111). Reprinted with permission from Majzik et al.[80] Copyright 2018, Springer Nature.

(D) Adsorption structure of the enantiomers of [123]tetramantane on Cu(111) (blue, H; red, C). Reprinted with permission from Ebeling et al.[92] Copyright 2018, Springer Nature.

(E) Experimental and calculated forces between the tip-terminating CO molecule and the Fe atom anchored on Cu(111). Reprinted with permission from Huber et al.[93] Copyright 2019, The American Association for the Advancement of Science.

Some other factors of the metal/metal oxide substrates also influence the molecular adsorption. First, the lattice of the substrate can guide the adsorption site and direction of the molecules (or atoms).[23,90] Second, the lattice match degree of the molecule and the substrate plays an important role. For example, 4,4″-diamino-*p*-terphenyl adsorbed on Cu(111) in an asymmetric manner while on Au(111) the symmetry was well maintained (Figure 5B).[91] Third, when metal oxide substrates are used, the surface structure and the oxygen termination may also affect the adsorption configuration.[94]

The interaction between the molecule and substrate can be weakened by depositing an inert NaCl film onto the metal surface, making the target molecule much closer to a free one and leading to different structure and properties.[18] As shown in Figure 5C, in contrast to the open-shell configuration of the indeno[1,2-*b*]fluorene molecule adsorbed on Cu(111), a closed-shell configuration with antiaromaticity was observed on a bilayer NaCl-covered Cu(111).[80] However, there are also cases where the molecules are bound to the NaCl thin film via the interaction between the molecule and Na^+ or Cl^- in NaCl.[95] Therefore, the molecule-substrate interaction should be analyzed case by case.

In addition, owing to the high resolution of sm-AFM, the on-surface chirality of the adsorbed molecules can be facilely identified,[49,92,96,97] which effectively addresses the issue of difficult assignment of enantiomers without chromophores in conventional techniques. Ebeling et al.[92,96] revealed the enantiomers of [121]tetramantane and [123]tetramantane successively. The adsorption structures of [123]tetramantane are shown in Figure 5D, where the features of two top H atoms could be clearly seen.[92] Namely, in the (M)-type molecule the top H atoms locate at the right side above the Olympic ring, while in the (P)-type molecule they are at the left side,

thereby the enantiomers of [123]tetramantane can be easily distinguished. Furthermore, advanced sm-AFM also enables the elucidation of the pathway of enantiomer interconversion.[49]

As well as the above-discussed molecular adsorption on the substrate, the interaction between the tip-terminating CO and the target molecule/atom is another important aspect. Both physisorption and chemisorption may exist. For example, the Si atom shows a physisorption state with CO while the Cu atom interacts with CO via chemisorption.[93] Interestingly, when imaging the Fe atom, a transition from physisorption to chemisorption was found. The experimental force versus distance curve is shown in Figure 5E, where a physiosorbed force minimum at 420 pm is followed by a maximum chemisorbed attractive force at 250 pm, with a force barrier of +17 pN at 310 pm. The top-view force map at a constant height of 280 pm also reveals the transition from van der Waals attraction to Pauli repulsion and then to attraction again, from middle to sides, in good agreement with the calculated results. Similar phenomena have also been demonstrated in Fe clusters in a very recent study.[98] These works indicate that the CO molecule adsorbed on the tip might not be chemically inert, so the observed structure and properties must be prudently explained.

3D molecules

Accurate visualization of 3D molecules remains a great challenge. In the typically used constant-height scan, different parts of the 3D molecule will produce different atomic contrasts due to the different distances to the tip, making it hard to interpret the molecular structure.[54,96,99] The background force resulting from the surrounding atoms and the flexibility of the tip-terminating CO molecule further limit the precision of imaging. Moreover, an undesirable contact between the tip and the target molecule may occur, causing contamination and even destruction of the tip.

So far, five approaches have been developed to image molecules with 3D configurations. First, separately scan different parts of the molecule at different heights.[96,100] Second, apply a custom height profile for imaging.[92] Third, combine with mapping in a plane perpendicular to the sample surface.[101] Fourth, use a two-pass imaging mode.[54] Namely, the molecular topography is recorded in the first pass, where parameters are optimized via the tip-molecule distance feedback, while the preset height profile is followed in the second pass in an open feedback loop with parameters optimized to realize high resolution. Fifth, as an improvement of the fourth approach, utilize the tunneling current to track the molecular topography and meanwhile record the frequency shift to achieve atomic contrast.[99] Of these approaches, the first is less preferred since it is laborious, while the fourth and fifth approaches are most promising for accurate 3D molecule imaging.

Furthermore, a recently developed machine learning method based on a deep convolutional neural network achieved the reliable and rapid interpretation of sm-AFM images of complicated 3D molecules.[102] This model can accurately identify molecular adsorption configurations, which significantly reduces the possible solutions of molecules from a series of sm-AFM images. Nevertheless, further studies are highly desirable, mainly to add more atoms to the training set, improving the model robustness, including non-spherical electrostatics and molecular displacements in the model, etc.

Intermediate species

Owing to the stabilization effect of the low temperature used in sm-AFM, the reactive molecules can be frozen, enabling the image capturing of the intermediate

species, from which the pathway of the chemical/physical processes can be revealed. Compared with generally used diffuse reflectance infrared (IR) Fourier transform spectroscopy, nuclear magnetic resonance spectroscopy, isotope tracer, etc., this approach provides a direct route toward a deep mechanistic understanding down to the atomic level.

The pathway of the on-surface reactions has been identified by sm-AFM. Radicals, as the most common intermediates, are generally formed in tip-induced on-surface reactions,[19,89,97] and also in some thermally induced cases.[103] Despite the high chemical instability of the radicals due to unpaired electrons, the chemical structure and even the dissociation and rearrangement of the radicals on the surface have been visualized via sm-AFM.[89,97,100] For example, as shown in Figure 6A, induced by the voltage pulse, 9,10-dibromoanthracene lost two Br atoms successively to form 3,4-benzocyclodeca-3,7,9-triene-1,5-diyne, during which two radicals, namely, non-planar 9-dehydro-10-bromoanthracene monoradical and planar 9,10-didehydroanthracene diradical, were clearly resolved.[21]

In contrast, identification of the intermediate species in thermally induced on-surface reactions is more complicated. The reaction must be quenched because a cooling process down to ~5 K is indispensable for high-resolution sm-AFM imaging.[7,85,100,104] Figure 6B illustrates the pathway of the Ullmann reaction from bromotriphenylene to bistriphenylene through a triphenylene radical and an organometallic intermediate, which were demonstrated using separate heating procedures.[100] The statistical analysis of the substances at different temperatures (Figure 6C) further demonstrated this pathway. Here, such a statistical approach is reliable and accurate, which should draw more attention for reaction pathway exploration.

Seeing how a physical process occurs can be even more interesting. Very recently, the intermediate edge structures involved in the growth of 2D bilayer water networks were successfully captured by real-space sm-AFM imaging, by which the growing process was revealed.[8] The structure of the water network was discussed in Molecular structure. Here, the zigzag and armchair edges showed distinct growing mechanisms. As shown in Figure 6D, the growth of a zigzag edge was achieved by forming a periodic pentagon array (steps 1–3) and their subsequent bridging into a 56665-type structure (step 4). In contrast, for the armchair edge (Figure 6E), the 575-type rings were converted into 656-type rings by two water pairs (steps 1 and 2), followed by the lateral growth to form a 5656-type edge (step 3). Due to the strain accumulation, the length of the 5656-type edge was restricted, which can be partially released by adding a water pair into the hexagon (step 4), turning back to the initial 575-type structure. Such a process involves local seeding and edge reconstruction, and thus is less efficient. This great work challenges the conventional thought and should inspire more efforts into growth of water/ice.

Molecular mixture

sm-AFM is a powerful tool to detect, identify, and quantify the individual molecules in a complex mixture. Not only the multiple products in a chemical reactions but also the naturally occurring mixtures, such as petroleum, have been discriminated via sm-AFM. In contrast to conventional techniques that just give an ensemble property, sm-AFM allows the exact molecular identification of each component, and the relative proportion of those components can be obtained via statistical analysis. In general, acquiring an atomically resolved sm-AFM image takes about 10 min, which limits the imaging molecule number to a few hundreds.[31]

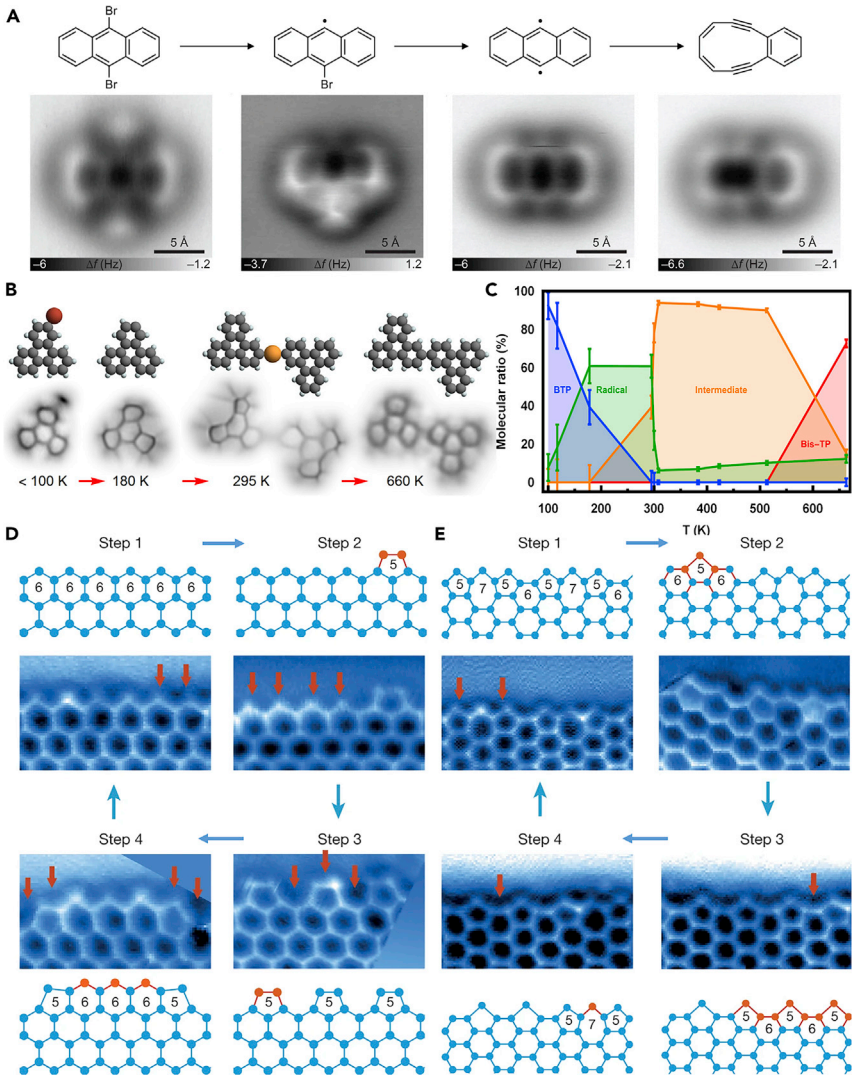

Figure 6. sm-AFM images and corresponding models of the precursor, intermediate species, and product in on-surface chemical and physical processes

(A) Bergman cyclization reaction induced by voltage pulses. Reprinted with permission from Schuler et al.[21] Copyright 2016, Springer Nature.

(B and C) (B) Ullmann reaction induced by thermal energy (white, H; gray, C; brown, Cu), and (C) corresponding statistical analysis of substances. Reprinted with permission from Zint et al.[100] Copyright 2017, American Chemical Society.

(D and E) Growing process of a 2D bilayer water network at (D) zigzag edge (image size, 3.2 × 1.9 nm) and (E) armchair edge (image size, 3.7 × 2.2 nm). Red arrows suggest the addition of one bilayer water pair, which will lead to the structure in the following image, while red balls and sticks represent the newly formed bilayer water pairs. Reprinted with permission from Ma et al.[8] Copyright 2020, Springer Nature.

In 2015, Gross and coworkers[105] first utilized sm-AFM to reveal the constituents of one of the most complex natural mixtures, asphaltene. Surprisingly, the constituent molecules of both petroleum- and coal-derived asphaltenes were found to be larger than previously expected. Moreover, very recently, the semicentennial structure puzzle of the petroleum pitch was explored at the molecular level.[106] A wide range of cata- and peri-condensed polycyclic aromatic hydrocarbons (PAHs) with a few short alkyl chains and/or five-membered alicyclic rings constitute the petroleum

pitch M-50. More importantly, the single-core and multi-core architectures were demonstrated to simultaneously exist, contradictory to the widely held belief of the presence of only one type.

Furthermore, a novel multidisciplinary methodology integrating sm-AFM with other analytical tools has been developed for identifying and quantifying new PAHs.[107] Four steps are involved. First, identify an unknown PAH via sm-AFM. Second, synthesize this PAH. Third, confirm the molecular structure of the synthesized PAH via sm-AFM. Fourth, analyze this PAH by liquid chromatography/UV-vis spectroscopy. This method has been demonstrated to be effective for the pyrolysis products of *n*-decane, which in essence provides a reliable reference for subsequent analysis.

Spin and magnetic properties

As an extension of sm-AFM, the spin and magnetic properties of molecules can be detected by adsorbing a magnetic molecule Ni(cyclopentadienyl)$_2$ ($NiCp_2$) onto the tip.[32,33] The $NiCp_2$ molecule retains its S = 1 spin triplet ground state when adsorbed on the Cu tip, thus being able to serve as a molecular spin sensor. The strength of the exchange interaction (E_{ex}) can be probed and mapped via changes in the spin excitation spectrum of $NiCp_2$, revealing atomic-scale regions where the quantum states of the tip and the target molecule strongly mix with each other.[32,33] So far, the exchange field and spin polarization of $NiCp_2$ molecule,[32] Fe atom,[33] and Co film,[33] have been elucidated. Furthermore, the simultaneous excitation of spin and vibration quanta was revealed with single $NiCp_2$ molecules, providing a new route for identifying the pathway of spin relaxation.[108]

Such an advanced technique allows the regulation of spin state, spin coherence lifetime, as well as the direction and magnitude of magnetic anisotropy, etc., simply by tuning the sensor functionality.[32,109] For example, reproducible Kondo resonance can be generated and regularized by tip functionalization with single Co(cyclopentadienyl)$_2$ ($CoCp_2$) and Co(isoindole)$_4$ (CoPc) molecules, respectively.[110,111] As an analog of the force-sensing CO-functionalized tip for structural imaging, the spin-sensing $NiCp_2$ ($CoCp_2$ or CoPc)-terminated tip will undoubtedly be widely adopted in the near future for atomic-scale spin and magnetic research, accelerating the development of signal transmission, digital data storage, catalysis, drug delivery, cancer therapy, etc.

Electronic properties

sm-AFM mainly probes the total electron density distribution. To get more information about charge distribution and molecular orbitals, other techniques, such as KPFM[112] and STM,[24,48,113] are needed. In this subsection, we briefly discuss these supplementary techniques, with which a comprehensive overview of the electronic properties of the target molecule can be obtained.

Charge distribution is generally analyzed via the electrostatic field of the molecule. KPFM, as an offspring of sm-AFM, is capable of reflecting the charge state and charge distribution by recording the external voltage applied to get the maximum frequency shift (minimum electrostatic field) at each site.[114] The major difference between sm-AFM and KPFM lies in the fact that, while sm-AFM is mainly based on short-range forces, KPFM relies on long-range electrostatic forces.[115,116] KPFM is particularly useful for element identification, which is difficult to be realized by sm-AFM.[74] Furthermore, the exploitation of KPFM also enables the study of the charge distribution of the tip for a better understanding of the sm-AFM results.[117] In addition, the operando KPFM has been increasingly used as a powerful tool to

investigate surface defects, adsorption state, and energy band structure, as well as charge transfer, polarization, and trapping, thus showing a broad application in catalysis, solar cells, sensors, microelectronics, etc.[116,118–120] For example, the catalytic reactivity of Pd nanoparticles dispersed on a highly oriented pyrolytic graphite surface was revealed by KPFM based on the changes in work function.[118] However, a chemical bond is formed within such a small tip-molecule distance, thus lowering the accuracy of the data. Recently developed scanning quantum dot microscopy (SQDM), which utilizes the quantum dot to detect and image the electrostatic potential, effectively addresses this issue.[121] The screening effect of the tip-molecule system causes an exponential decay of the electrostatic potential with the lateral distance from the tip, leading to a high resolution for quantitative imaging of the surface potential. Also, owing to the single-molecule sensitivity and the vibrational Stark effect, tip-enhanced Raman scattering-relayed molecular force microscopy (TERS-MFM) can realize the accurate imaging of the electrostatic field as well.[122]

Molecular orbitals, particularly the highest occupied molecular orbital (HOMO) and the lowest unoccupied molecular orbital (LUMO), are an important aspect of the structural and electronic properties. Typically, molecular orbitals (mainly HOMO and LUMO) are resolved via STM by applying a voltage between the tip and the target molecule and then measuring the tunneling current.[123] The constant-current mode is generally used with adjustable tip height. Combined with scanning tunneling spectroscopy, the local density of states of the sample can be facilely obtained.[58,78] Also, the positive and negative ion resonances derived from HOMO and LUMO can be visualized, and the energy gap can be quantitatively extracted.[48] Furthermore, the singly occupied molecular orbital of a radical, and even its nodal plane structure, can be probed by mapping the spatial distribution of Kondo resonance.[124] However, the use of the conductive substrate for STM imaging inhibits the redox-state transitions.[113] Fortunately, this has recently been solved by synchronizing short voltage pulses (to steer electron tunneling) with cantilever oscillation at the resonance frequency, leading to a novel single-electron alternate-charging STM technique.[113] As a result, the influence of electron transfer and polaron formation on molecular orbitals was successfully visualized.

Coupling sm-AFM with other techniques

Besides STM, KPFM, SQDM, and TERS-MFM, which were discussed in Electronic properties, IR and Raman spectroscopy could also be coupled with sm-AFM to obtain more information about the chemical composition down to the atomic scale.[122,125–127] In sm-AFM-IR, a tunable IR laser is focused on a region of the sample right below the sm-AFM tip. When IR light with the characteristic wavelength is absorbed, thermal expansion results, leading to a force impulse on the sm-AFM tip. Thereby, the absorption wavelength of the sample can be mapped.[125] Here, the resolution is determined not only by the sharpness of the sm-AFM tip but also by the focal spot size of the IR laser.

The technique combining sm-AFM and Raman spectroscopy is known as TERS. While AFM-IR relies on IR light absorption, TERS measures the light scattering, with an emphasis on the use of a field-enhancing metal tip to enhance the Raman-shifted light scattered from the small region below the tip because of the excitation of surface plasmons.[127] Furthermore, equipping pulsed excitation sources for TERS is highly expected to achieve both ultrafast temporal and ultrahigh spatial resolutions.[128] From the other perspective, when a CO molecule is adsorbed on the tip, TERS could optically relay its vibration signal, by which the structure and charges of the sample can be revealed.[122] Integrated characterization techniques will

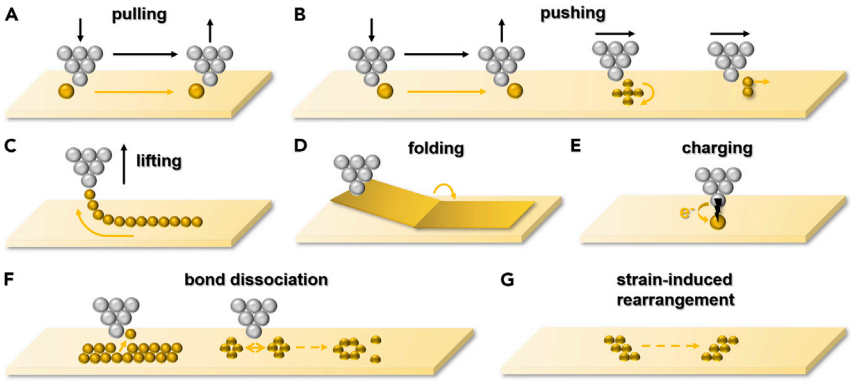

Figure 7. Schematic types of atomic manipulation
(A) Pulling.
(B) Pushing.
(C) Lifting.
(D) Folding.
(E) Charging.
(F) Bond dissociation.
(G) Strain-induced rearrangement.

undoubtedly deepen our understanding of emerging materials and further promote their wide application.

MANIPULATING SINGLE MOLECULES/ATOMS

There are seven manipulation types, as illustrated in Figure 7, namely, pulling, pushing, lifting, folding, charging, bond dissociation, and strain-induced rearrangement. Pulling, lifting, and folding rely on the attractive interaction between the tip and the molecules/atoms, whereas pushing is realized with the repulsive interaction. Charging results in the switching of the charge state by electron attachment and detachment, while tip-induced bond dissociation involves the removal of atom(s) and subsequent atomic rearrangement or intermolecular coupling. Atomic rearrangement may result because of substrate-induced strain as well. In this section, each type of manipulation will be thoroughly discussed from the perspective of manipulation principle and application. STM manipulation is included as needed, since it is generally coupled with sm-AFM.

Pulling

Single molecules/atoms can be pulled by the tip (either with or without single-molecule functionalization), owing to the attractive interaction between them (Figure 7A). As early as 1990, IBM researchers realized the movement and arrangement of Xe atoms into an IBM logo on Ni(110).[129] This was achieved via the following four steps. First, use imaging mode to find the position and destination of the target atom. Second, lower the tip toward the atom by increasing the tunneling current in a closed loop. Third, move the tip to the desired destination across the surface while dragging the target atom. Fourth, withdraw the tip by decreasing the tunneling current. What is even more impressive, in 2013, using a similar technique, IBM researchers created the world's smallest movie entitled *A Boy and His Atom*, by moving CO molecules with a Cu tip to generate images and then assembling them into a film. Stimulated by these excellent works, some interesting atomic patterns and physical phenomena have been created and discovered.[130,131]

The interaction between the target molecule/atom and the substrate plays an important role for atom movement, since it directly determines the moving resistance.[130,132] In general, a stronger interaction requires a larger pulling force and thereby a smaller tip-atom distance. This allows us to quantitatively investigate the atomic-scale friction force and the diffusion barrier.[132,133] However, it should be noted that the attractive interaction between the tip and the target molecule/atom can lower the diffusion barrier, thus leading to a smaller threshold force compared with that obtained from the lateral derivative of surface potential.[134] In addition, elevating the temperature can thermally assist the dragging process by lowering the threshold force.[135] While a larger pulling force enables a continuous sliding behavior with a constant tip-atom distance, a smaller pulling force can only make the target molecule/atom perform hops to follow the attractive tip.[130,132,135]

Furthermore, recently, long-distance pulling has been exploited to investigate the interfacial transport of Na^+ hydrates.[136] Namely, with the assistance of hot electrons for activation, *in-situ*-fabricated Na^+ hydrates diffused toward the Cl^--functionalized tip on a NaCl(001) surface because of the electrostatic attraction. Interestingly, Na^+ hydrated with three water molecules showed the highest diffusion rate, which is orders of magnitude higher than others. This provides an atomically precise method for studying interfacial molecular diffusion.

Pushing

In general, large molecules are preferentially moved via pushing, in contrast to the manipulation of single atoms where pulling is preferred. While the pulling mode relies on the attractive interaction, pushing a molecule works via repulsive interaction: within a small tip-molecule distance, the wave function of the molecule overlaps with that of the tip, generating repulsive force to push the molecule across the surface and, in some cases, cause the tilting of the vertically aligned molecule[40,137] or rotate the molecule (Figure 7B).[138] Typically, pushing is achieved with a molecularly passivated tip, which exhibits an evidently suppressed interaction with the target molecule.

Pushing a molecule is prone to cause its destabilization due to the high degree of mechanical freedom. Therefore, when targeting at moving a molecule along a certain direction, a highly anisotropic substrate is desired to confine the adsorption of the target molecule.[130] The orientation, length, and position of the path must be properly defined to avoid complex manipulation patterns. Moreover, the occurrence of the relaxation of the molecule or tip, which can be reflected in the frequency shift curve, should be carefully dealt with. If the pushing force is not large enough or the molecule-substrate interaction is very strong, the molecule cannot be moved; instead, it can only be tilted, particularly for vertically aligned molecules.[40,137]

From another perspective, pushing serves as an effective way to reversibly switch a molecule between its bistable states, showing a great promise for molecular devices, such as binary memory.[138,139] Intriguingly, pushing can induce the molecular domino effect, enabling the transfer of intermolecular signals.[138] This was achieved via the rotation of a set of dichlorotin phthalocyanine molecules or, in other words, the transition between their α and β forms on the Cu(110) surface. Furthermore, very recently, directly exerting a femtosecond atomic-scale force on individual atoms was achieved with the near field of a terahertz wave, enabling coherent molecular rotation.[13] This great breakthrough paves the way for controlling the chemical reaction and physical phase transition on their internal spatiotemporal scale.

Lifting

Lifting requires the attractive interaction between the tip and the sample (either single molecules or atoms), which can originate from the intrinsic properties of the tip and sample (to form chemical bond),[140] or be assisted by external voltage.[12,16,90,141] For larger molecules, the anchoring site must be predefined, the interaction of which with the tip apex must be strong enough to overcome the adhesion and friction forces between the molecule and the substrate. Moreover, a high stiffness and a small oscillation amplitude of the tip are desired to avoid abrupt rupture when removing the sample from the substrate.[140]

The earliest and most widely applied form of vertical manipulation is to pick up a single atom or molecule to functionalize the tip. Moreover, in some cases, the atom or ion is picked up by the tip and then implanted into a desired location for controllable atomic manipulation and corresponding property investigation.[142] Beyond these, lifting larger molecules (generally 1D molecules) off the substrate is an effective approach for conductance measurement (Figure 7C).[12] The operational procedure is as follows. First, approach the tip to the predefined anchoring site of the target molecule. Second, retract the tip to lift the molecule with the tunneling current being recorded. Third, release the molecule by applying a pulse voltage. The evolution of the current with the moving distance implies the mechanism of charge transfer, while the slope in the logarithmic plot, defined as the decay constant β, reflects the effective mass of charge carriers, bandgap, and energy level alignment.[12,143] Using this method, and integrating it with some improvements, the electrical properties of several 1D materials have been revealed.[12,16,90]

Furthermore, lifting enables the evaluation of the mechanical properties of these 1D molecules. The easiest way is to compare the molecular structures before and after lifting and releasing to see if there is breakage or deformation. Moreover, the molecular friction can be quantitatively investigated by lifting and sliding the molecule on a certain surface. For example, as shown in Figure 8A, a graphene nanoribbon was oscillated back and forth on a Au(111) surface at a constant tip height, during which a fluctuation of the frequency shift of the tip was observed with a periodicity of 0.28 nm.[9] Here, the period represents the length of the repeating unit, while the jump is caused by the detachment of each unit.[144] This kind of pattern indicates a nearly frictionless motion expected for stiff 1D molecules. Moreover, while the surface properties affect the dynamics of sliding motion at a small tip height, the influence of the bending properties of the suspended part of the molecule dominates upon increasing the tip height.[9]

Lifting a molecule to make it stand upright requires a more delicate design, with an emphasis on the choice of the pedestal and lifting trajectory.[10,145] Most attractively, an atypical and surprisingly stable standing single-electron field emitter was fabricated by Tautz and coworkers in 2018.[10] This was achieved by connecting two Ag atoms (as the pedestal) with a 3,4,9,10-perylenetetracarboxylic-dianhydride molecule and then retracting the tip along a customized trajectory. This trajectory mimicked peeling an adhesive from a plate with the far end kept stationary in the first stage, followed by vertical lifting (Figure 8B). This standing molecule never fell back to the surface by itself and could maintain the vertical configuration even at a high current density of 10^8 A/m^2. Such a unique structure enables cascading of the charging of the quantum dot and single-electron field emission.

Furthermore, with the realization of controllable vertical manipulation of single molecules, the first case of electrostatic catalytic non-redox reaction was achieved.[11] As

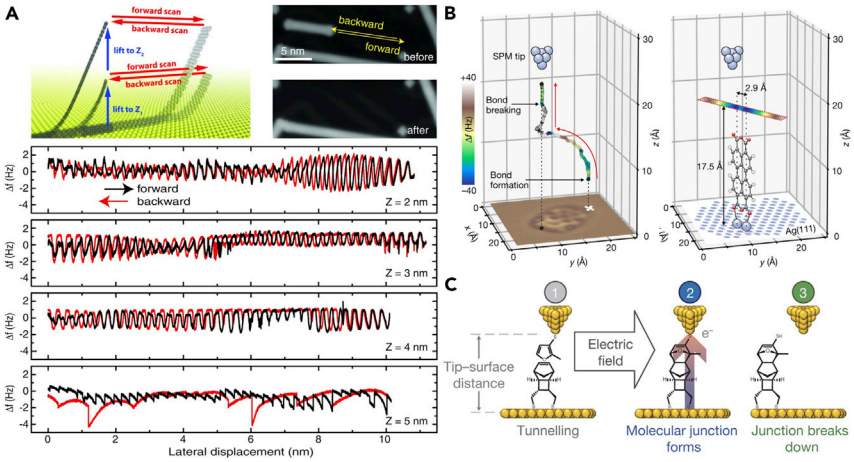

Figure 8. Vertical manipulation of single molecules

(A) Friction measurement by lifting and sliding graphene nanoribbon. Reprinted with permission from Kawai et al.[9] Copyright 2016, The American Association for the Advancement of Science.

(B) Creation of a standing single-electron field emitter. Left: 3D trajectory used to lift 3,4,9,10-perylenetetracarboxylic-dianhydride molecule. Right: side view of the standing field emitter with two Ag atoms as the pedestal (white, H; gray, C; red, O; blue, Ag). Reprinted with permission from Esat et al.[10] Copyright 2018, Springer Nature.

(C) Electrostatic catalysis of a Diels-Alder reaction. Reprinted with permission from Aragonès et al.[11] Copyright 2016, Springer Nature.

shown in Figure 8C, the electric field stimulus was delivered across the pre-lifted diene adsorbed on the tip to the dienophile standing on the Au substrate, leading to the enhanced formation rate of single-molecule junctions up to 5-fold when the electron flew from dienophile to diene. This is because of the electrostatic stabilization effect on the minor resonance contributor of transition state.[11] Stimulated by this impressive work, utilizing a similar configuration, a number of studies on single-molecule reactions and single-molecule electronics have been conducted in the last 3 years.[146,147]

Folding

Folding is an emerging atomic-scale manipulation approach for 2D materials (Figure 7D). Groundbreakingly, in 2019, precisely folding and unfolding nanographene with controllable twisting angles was achieved by Chen et al.[17] Namely, the tip which attracted the nanographene edge via the tunneling junction moved across the nanographene plane and stopped at the predefined location, resulting in a folded nanographene with a dihedral angle up to 60° with a 0.1° accuracy. Folding and unfolding can be repeated several times without any structural defects or damages. Interestingly, folding the single-crystal nanographene created a tubular edge with specified chirality and 1D electronic properties that resemble those of carbon nanotubes, while folding the bicrystal nanographene resulted in well-defined intramolecular junctions. Such a novel atomic-scale origami is expected to be used for other 2D materials to reveal their potential magic physical properties.

Charging

The tip can induce the switching of the charge states of atoms or molecules by electron attachment and detachment. Charging can be achieved either locally by applying a voltage ramp on an insulating substrate,[14,112] or remotely by injecting hot carriers into the surface state of the metal substrate[148] or by surface polaron transfer.[149] Local charging is widely used where the ionic relaxation of the insulating

substrate (typically, NaCl film) can help to stabilize the charge states, with certain influence imposed by the substrate thickness.[112] Typically, a thick insulating substrate inhibits electron exchange thus resulting in multiple charge states and allowing the determination of reorganization energies.[14] Furthermore, subtly, the vibration of the sm-AFM tip can be coupled with the periodic switching of the charge state, shedding light on the electronic states of the molecule and its coupling with the substrate.[150]

Charging can lead to the change of the molecular conformation,[14] adsorption geometry,[149] bond-order relation,[14] aromaticity,[14] and molecular vibronic mode,[151] as demonstrated via sm-AFM. In 2019, Fatayer et al.[14] conducted a comprehensive study on the influence of charge states by ramping the bias voltage. First, the conformation change was demonstrated on azobenzene, where single-electron injection induced a reversal of the tilting direction of one of the phenyl rings (Figure 9A). Second, the adjustment of the bond-order relations was revealed with tetracyanoquinodimethane, where the anion showed bond order alternation while the bonds of the central ring in dianion were homogeneous (Figure 9B). Third, charging altered the adsorption geometry of pentacene where an evident elongation along its long axis was observed with the increase of the negative charge (Figure 9C). Fourth, the charge-state-dependent shift of aromaticity and macrocyclic conjugation pathway were identified on porphine (Figure 9D).

Furthermore, the local electric field of the tip enables the controllable manipulation of atoms buried under the surface, which cannot be achieved by common force- and tunneling current-based techniques.[15] As shown in Figure 9E, the application of an electric field (>1.2 V) realized the manipulation of a near-surface O atom in a high-temperature superconductor $Bi_2Sr_2CaCu_2O_{8+x}$, accompanied with a shift of surface biatoms.[15] The gap maps before and after the electric field-induced manipulation of ~10 O atoms showed significant gap variations above 10 meV (Figure 9F), which is directly reflected in the difference map (Figure 9G). Moreover, reversal of the surface modification by electric field treatment can revert the gap back. This excellent work demonstrates an approach to reversibly and nondestructively probe the effect of local lattice on the electronic state.

Bond dissociation

Tip-induced bond dissociation and subsequent skeleton rearrangement is the representative of on-surface reactions, allowing the investigation of every single step of the chemical reaction down to the atomic scale. Bond dissociation is achieved by energy transfer from the tip to the target molecule, which is generally within a few electronvolts based on the bond enthalpies. Varied by the studied systems (including the substrate), energy is transferred to the vibrational mode or the electronic resonance state of the target molecule, resulting in different threshold voltages (energy barrier divided by electron charge).[152] As long as the energy barrier is overcome, the molecule will undergo chemical transformation. Typically, to make the process energy efficient, temporary electron attachment by applying a pulse voltage is preferred. Here, it should be noted that not all the target atoms can be removed since there is an energy tradeoff between bond dissociation and molecular degradation.[153]

Dehydrogenation is one of the most widely used approaches in organic synthesis. A series of acenes have been synthesized on Au(111) by abstracting H atoms with the tip placed above the methylene groups and with the voltage being larger than the LUMO energy up to 2.5 V (Figure 10A).[47] A similar operation for hydrogen abstraction has been used to synthesize triangulene,[22] indeno[1,2-*b*]fluorene,[80] etc. The

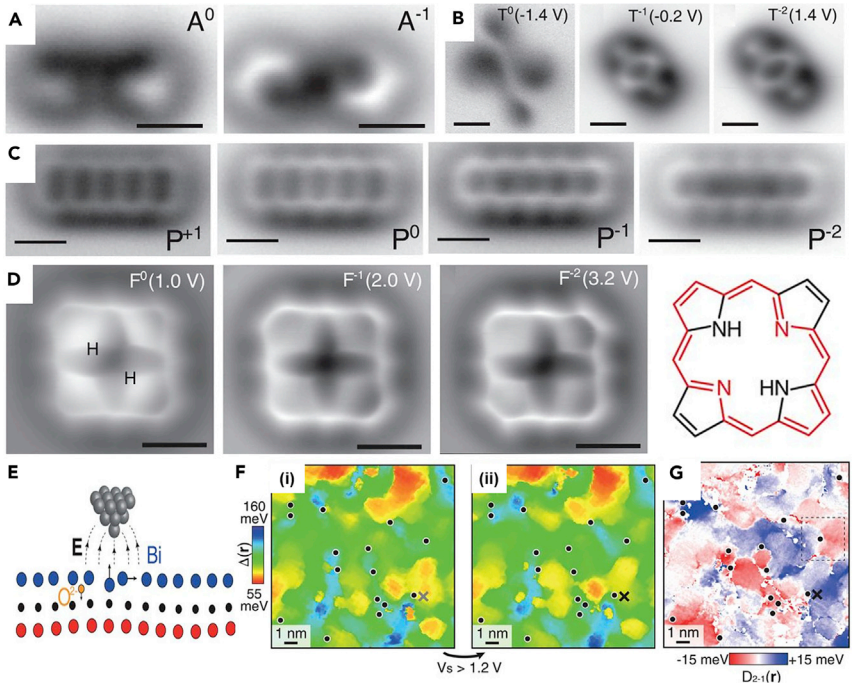

Figure 9. Molecular structures and properties with different charge states

(A) Conformations of azobenzene.

(B) Bond-order relations of tetracyanoquinodimethane.

(C) Adsorption geometries of pentacene.

(D) Aromaticity of porphine. Scale bars represent 5 Å. Reprinted with permission from Fatayer et al.[14] Copyright 2019, The American Association for the Advancement of Science.

(E) Schematic charge-induced atomic manipulation of $Bi_2Sr_2CaCu_2O_{8+x}$.

(F) Peak-to-peak gap maps before and after manipulation.

(G) Difference map of the peak-to-peak gap (dots represent the locations where biatoms are manipulated). Reprinted with permission from Massee et al.[15] Copyright 2020, The American Association for the Advancement of Science.

removal of H atoms induces the rearrangement of the intramolecular skeleton and sometimes planarization and lateral displacement of the molecule.[22] Very recently, tip-induced dehydrogenative intramolecular coupling of terminal alkynes was demonstrated on NaCl with a voltage larger than 4.5 V (Figure 10B), in which the abstraction of the second H atom took place after the formation of a C-C bond.[154]

The bond enthalpies of C-X bonds (X denotes halogens, such as Br and I) are smaller than that of the C-H bond, thus requiring less energy input for dehalogenation.[160] Moreover, applying an appropriate voltage will first remove the halogen atom (break the weakest C-X bond), by which the radical center can be predefined.[19,152] A number of dehalogenation reactions have been conducted on the NaCl surface, which is beneficial for resonant tunneling into LUMO and facilitates the vibrational excitation within the molecule, thus significantly lowering the threshold voltage.[152] Moreover, the chemically inert NaCl can prevent the reaction between the intermediate radicals and the substrate. For example, tip-induced stepwise debromination and subsequent Fritsch–Buttenberg–Wiechell rearrangement on NaCl surface have been demonstrated for polyyne synthesis (Figure 10C).[19] Similarly, kicking out Br atoms also enabled the preparation of cyclo[18]carbon,[53] meta-aryne,[152] and 3,4-benzocyclodeca-3,7,9-triene-1,5-diyne,[21] where the removal of the second Br atom typically requires a higher voltage. On the other hand, metal substrates have

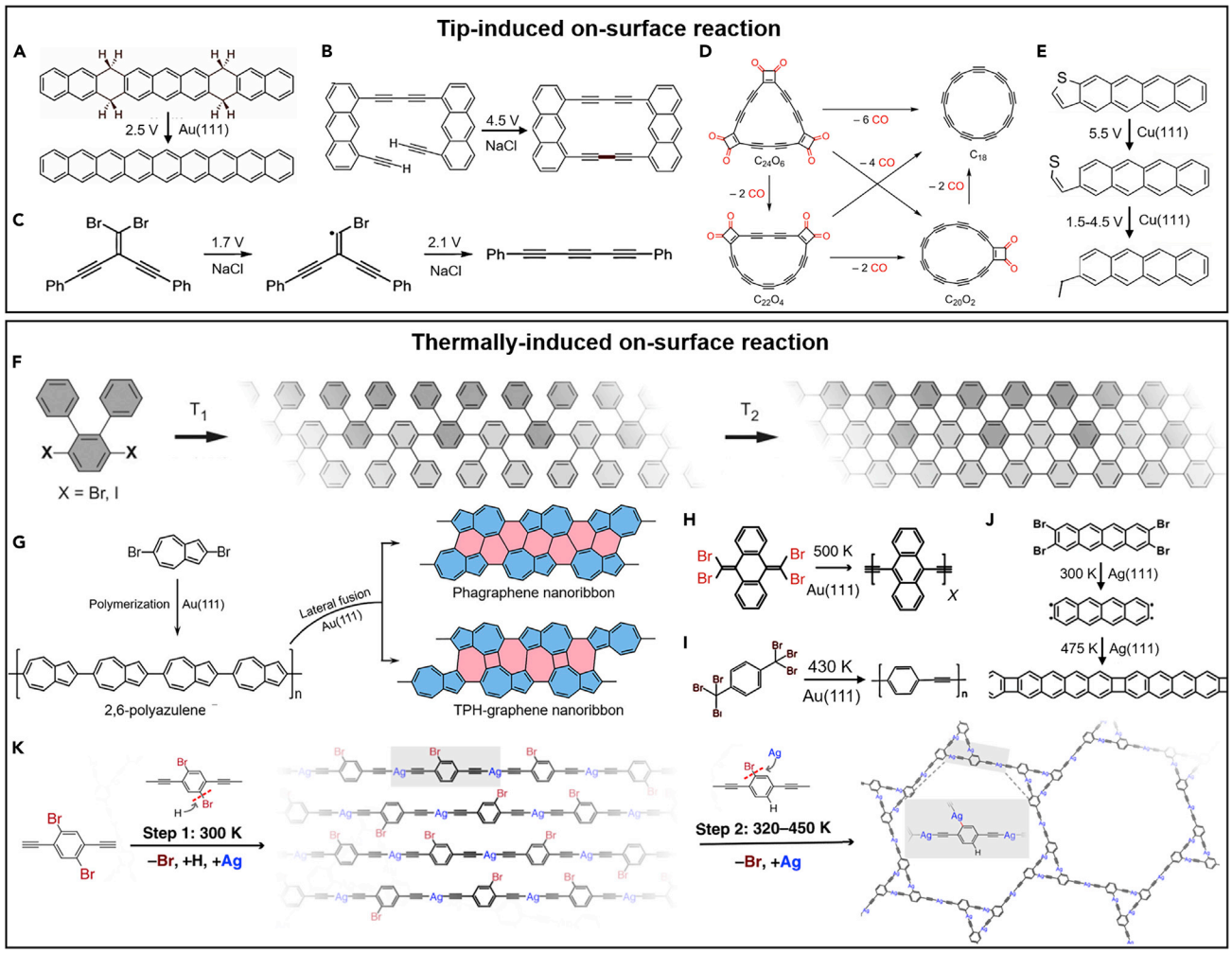

Figure 10. Tip-induced and thermally induced on-surface reactions

(A–E) Tip-induced: (A) dehydrogenation. Reprinted with permission from Zuzak et al.[47] Copyright 2018, Wiley-VCH Verlag GmbH & Co. KGaA. (B) Dehydrogenative intramolecular coupling. Reprinted with permission from Albrecht et al.[154] Copyright 2020, Wiley-VCH Verlag GmbH & Co. KGaA. (C) Debromination and subsequent Fritsch–Buttenberg–Wiechell rearrangement. Reprinted with permission from Pavliček et al.[19] Copyright 2018, Springer Nature. (D) Decarbonylation for cyclo[18]carbon synthesis. Reprinted with permission from Kaiser et al.[18] Copyright 2019, The American Association for the Advancement of Science. (E) Desulfurization via applying electric field. Reprinted with permission from Borca et al.[146] Copyright 2017, American Chemical Society.

(F–K) Thermally induced synthesis of: (F) graphene nanoribbon via dehalogenation and cyclodehydrogenation ($T_1 < T_2$). Reprinted with permission from Giovannantonio et al.[155] Copyright 2018, American Chemical Society. (G) Non-benzenoid carbon nanoribbon via debromination and cyclodehydrogenation. Reprinted with permission from Fan et al.[156] Copyright 2019, American Chemical Society. (H) Anthracene (n = 3) polymer via debromination (removing four Br atoms). Reprinted with permission from Cirera et al.[24] Copyright 2020, Springer Nature. (I) Poly(arylene ethynylene) via debromination (removing six Br atoms). Reprinted with permission from Sun et al.[157] Copyright 2018, Wiley-VCH Verlag GmbH & Co. KGaA, Weinheim. (J) Tetracene-based nanoribbon via debromination (removing four different-position Br atoms). Reprinted with permission from Sánchez-Sánchez et al.[158] Copyright 2019, Wiley-VCH Verlag GmbH & Co. KGaA, Weinheim. (K) Organometallic 1D chains and 2D network via stepwise on-surface dissymmetric reaction. Reprinted with permission from Liu et al.[159] Copyright 2019, Springer Nature.

also been used for dehalogenation, which show a strong interaction with molecules and serve as the catalyst in some cases. After removing the halogen atoms, the unsaturated molecule tends to bind with the underlying metal substrate, which may further cause the tilting or twisting of the molecule.[52,89] Moreover, the radical formed by tip-induced debromination can be bromized again by releasing the Br atom adsorbed on the tip.[161] In addition, although less investigated, deiodination has also been reported.[20,89]

Besides dehydrogenation and dehalogenation, the tip can also induce decarbonylation,[18] deoxygenation,[153,162] and desulfurization,[146,163] with bias voltage applied. The most attractive example of decarbonylation is the creation of cyclo[18]carbon from $C_{24}O_6$ by removing six CO moieties under a bias voltage of 3 V on the NaCl surface (Figure 10D), which is mediated by inelastic electron tunneling by hot interfacial electrons.[18] Tip-induced deoxygenation, as another important manipulation technique, has enabled the reduction of vanadyl-phthalocyanine into the elusive vanadium-phthalocyanine,[162] as well as the removal of O atoms in tetraepoxycyclacenes.[153] Furthermore, selective desulfurization has been realized via locally injecting energy-tunable electrons into the resonant molecular states,[163] and by applying an electric field between the tip and the sample.[146] In the latter case, two C-S bonds were successively cleaved, where the first bond dissociation was barely activated by the electric field, while the second one was driven by the electric field with simultaneous electron injection (Figure 10E).[146]

Strain-induced rearrangement

The substrate can induce the strain for adsorbed molecules, which may further drive the on-surface reaction along a certain direction. This atomic-scale mechanochemical rearrangement has been recently demonstrated for several reactions. On the one hand, strain enables the controllable skeleton rearrangement of PAHs. For example, the large strain in two adjacent azuleno moieties of the diazuleno[1,2,3-*cd*:1′,2′,3′-fg]pyrene molecule drove the rearrangement of one azuleno moiety into a fulvaleno or naphtho moiety.[164] On the other hand, strain can induce the isomerization of 1D metal-organic chains.[103] Namely, the release of the substrate-induced strain made the metal-organic chain rearrange via 1,3-H shifts with the migration of the monomer backbone. More efforts are still desired to explore the mechanism underlying these strain-induced on-surface reactions.

THERMALLY ACTIVATING SINGLE MOLECULES

Besides molecular characterization and atomic manipulation, thermal activation of single molecules to create novel assemblies with real-space visualization is another important application of sm-AFM. In this case, sm-AFM serves as a "temperature-adjustable reactor" equipped with a "high-resolution camera" to capture the structural change of the molecules. By elevating the substrate temperature, molecules are woken up, allowing their diffusion and self-assembly.[31] In contrast to the tip-induced on-surface reactions, as discussed in Bond dissociation, thermal activation is advantageous for producing larger covalently bonded defect-free structures with certain repeating units, which requires the catalytic activity and sometimes the template effect of the metal substrate. Both the temperature and the nature of the substrate can affect the precursor reactivity, reaction pathway, selectivity, and structural quality of the final products.[104] The nature of the substrate includes its interaction with the target molecule, surface crystallographic orientation, and surface atomic structure. Meanwhile, the temperature imposes the kinetic control for on-surface reactions in terms of molecular diffusion, collision, reorganization, and desorption. After reacting for a certain time, the substrate must be cooled down to 5 K to acquire atomic-resolution images. This field has received great attention in the past decade and several great review articles have been published.[29,141] Therefore, here, we just briefly discuss the very recent advances in this booming field in terms of different reaction types.

Dehydrogenation and cyclodehydrogenation

Dehydrogenation and cyclodehydrogenation are effective approaches to planarize the non-planar molecules. In comparison with tip-induced dehydrogenation,

thermally induced dehydrogenation greatly enhances the reaction efficiency, thus generating an increased amount of target molecules.[47,165] This has been demonstrated on the preparation of acene molecules, where a 10-min annealing at 520 K resulted in almost 100% conversion, in great contrast to the trivial one-by-one atomic manipulation.[47] Moreover, interestingly, the introduction of additional atomic hydrogen, which could lead to the formation of radical intermediates, was demonstrated to be able to promote the dehydrogenation process.[166]

Compared with dehydrogenation, cyclodehydrogenation is even more intriguing since it has been widely applied to prepare π-extended PAHs (including graphene nanoribbons), and significantly improves their stability as well as the electronic conjugation of connections.[167] The reaction condition for cyclodehydrogenation is more intense than that for dehydrogenation, requiring a more reactive substrate or a higher temperature.[168] In such conditions, the cleaved H atoms can form H_2 molecules and then escape into the vacuum.[169]

Since the pioneering work in 2010, the most important application of thermally induced cyclodehydrogenation has been to prepare atomically precise graphene nanoribbons.[25] The bottom-up synthesis of graphene nanoribbons includes two steps (Figure 10F), namely, low-temperature polymerization (typically via dehalogenation, which is discussed in Dehalogenation) and high-temperature cyclodehydrogenation.[27,167] Cyclodehydrogenation is catalyzed by the metal substrate, which lowers the removal barrier of inner H atoms, since the van der Waals interaction between the substrate and the polymerized monomers favors the planar conformation.[170] Moreover, recently, using a similar method, nanoribbons of non-benzenoid graphene allotropes were created (Figure 10G), which paves the way for synthesizing novel carbon allotropes.[156] Smaller π-extended PAHs, such as triangulene,[50] coronoid,[59,60] and other nanographenes,[85] have also been successfully prepared with cyclodehydrogenation as an important step.

Dehalogenation

Dehalogenation is most widely used for on-surface synthesis of polymers and PAHs. The metal substrate serves as a catalyst, allowing a lower reaction temperature to inhibit the undesirable monomer desorption. The dehalogenation barrier generally decreases with the increasing reactivity of the metal substrate in the order of Au < Ag < Cu, while the barrier of deiodination is lower than that of debromination.[155] However, it should be noted that an excessively high reactivity of the substrate might lead to the formation of organometallic intermediates, while the one with an appropriate reactivity favors reversible dehalogenation.[171] After dehalogenation, the halogen atoms may remain adsorbed on the surface at temperatures up to 500 K.[81]

Dehalogenation is an effective approach for polymerization. Besides the common dehalogenative coupling with the formation of C-C single bonds, recently, C=C and C≡C interconnections have also been demonstrated with simultaneous abstraction of four halogen atoms, leading to the formation of 1D π-conjugated polymers (Figure 10H).[24,78,81] Impressively, dehalogenative coupling with six halogen atoms removed was also achieved, enabling the formation of C≡C bonds directly from sp^3-hybridized carbon (Figure 10I).[157] In addition, another interesting linker generated via dehalogenation is the cyclobutadiene moiety for acene nanoribbon by abstracting four Br atoms originally connected with different but adjacent C atoms (Figure 10J).[158] The synthesis of these atomically precise polymers with various linkers is a great breakthrough, since it has long been a huge challenge in conventional solution-based routes due to insolubility and/or high reactivity.

Furthermore, as mentioned in Dehydrogenation and cyclodehydrogenation, dehalogenation is always coupled with cyclodehydrogenation for π-extended PAH synthesis (Figures 10F and 10G).[155,156] In these cases, a large separation of the dehalogenation and cyclodehydrogenation temperatures is of vital importance since dehalogenation can be stopped by the H atoms generated in the cyclodehydrogenation step, forming C-H bonds at the unsaturated sites of radicals.[155] Moreover, the adsorbed halogen atoms generated during dehalogenation can combine with H atoms resulting from cyclodehydrogenation to form HX molecules. The detected HX molecules are utilized to mark the onset of the cyclodehydrogenation process.[172]

Organometallization

Organometallization has been observed in thermally induced on-surface reactions with the use of metal substrates, either as an intermediate step or directly forming the final product, which may exhibit as a small molecule, polymer, or network. In general, unsaturated molecules generated from dehydrogenation and dehalogenation can further form well-ordered metal-organic supramolecular structures on the metal substrate.[51,79,159,173] For example, as shown in Figure 10K, intermolecular coupling with H-passivation of one Br-substituted site at 300 K generated organometallic polymers, while subsequent heating at 320 K–450 K caused the other Br-substituted site to metalize and transformed these 1D chains into a 2D binodal network.[159] Here, the number and position of the functional groups influence not only the final molecular structure but also the reaction rate.[159]

In organometallization, the most important role of the metal substrate (e.g., Au, Ag, Cu, and Pt) is to directly take part in the reaction. If the coordinated metal atoms remain inside the metal surface, a tilted or bent adsorption geometry will be observed, while the planar adsorption configuration results from the lifted metal atoms.[100] In addition, the metal substrate serves as the catalytic template, driving the reaction at specific sites, aligning molecular growth along its crystallographic direction, and self-limiting the molecular size due to the strain accumulation, particularly for polymers.[174]

In some cases, further annealing at a higher temperature causes demetallization of the organometallic species with evidently shortened bonds identified.[51,100] However, there are also cases where post-annealing leads to the degradation of the molecules instead of demetallization.[52,174] This might be caused by the poor stability of the demetallized molecules, which are destroyed upon formation. So far, the mechanism and favorable conditions of demetallization remain unexplored, which should inspire more efforts into this mysterious field.

Other reactions

Over the past 3 years, thermally induced decarbonylation,[173] denitrogenation,[175] deoxygenation,[176] desilylation,[82] and C-C coupling[23,177] have been reported, further extending the application of on-surface reactions. Therein, desilylation is advantageous because the byproduct trimethylsilane is highly volatile, thus enabling a contamination-free on-surface reaction.[82] In this light, C-C coupling without any loss of atoms is even more attractive, where the metal surface not only directs the molecular assembly but also catalyzes the reaction.[23,177]

IMAGE SIMULATION

sm-AFM imaging is generally coupled with image simulation to demonstrate the molecular structure and, in some cases, to rationalize the imaging mechanism.

Currently, there are four main simulation approaches, which are discussed, with their pros and cons revealed, in this section.

Approximating the tip-sample force with interatomic potential is the simplest and most computationally efficient approach. The *Probe Particle Model* developed by Hapala et al.,[34] which describes the short-range and van der Waals interactions via pairwise Lennard-Jones potentials and combines them with a point charge or multipole interacting with the entire electrostatic field, has been widely used for sm-AFM image simulation. This model is capable of reproducing the experimental results and helping us to understand the origin of atomic contrast. However, the quantum force is transcribed to the classical force when constructing the interatomic potential, which might introduce simulation error or even failure, particularly when the tip is chemically reactive.[178]

Quantum mechanically treating the tip-sample-substrate system can give a much more accurate simulation, although it is computationally expensive.[178] The formalism can be applied to a variety of materials and well approximates the many-body interactions. However, this approach is so far severely limited by the size of the calculated system. Inspiringly, the booming electronic structure theories, such as the new eigensolver algorithm, are promising for reduction of the computational load.[178–180] Moreover, two approaches have been proposed to simplify the quantum model as described in the following.

In the *Virtual Tip* approximation, where the tip probes the electrostatic force of the sample, the tip is regarded as a classical object while the sample is treated quantum mechanically.[181] By treating the tip and sample differently, this approach effectively balances the simulation accuracy and the computational load. However, due to the simplification of the tip structure, this method is only suitable for inert single-atom tips, such as a Xe-functionalized tip, but fails for reactive and flexible tips.

In contrast to the *Virtual Tip* approach, the *Frozen Density* embedding theory treats the tip quantum mechanically and determines the force change by moving the tip within the fixed electrostatic field of the sample.[182] As a result, the size of the computational system is drastically decreased and thus the computational efficiency is greatly enhanced. The premise of this approximation is that, in non-contact sm-AFM imaging, the tip shows little influence on the electrostatic field of the sample.[182,183] Evidently, this approach cannot work under situations with strong tip-sample interactions.

SM-AFM FOR NEW MATERIAL—TAKING CYCLO[18]CARBON AS AN EXAMPLE

This century has witnessed a rapid development in new materials, and sm-AFM is considered to be the most powerful tool for material investigation. In this section, taking one of the most promising single-molecule materials, cyclo[18]carbon, as an example, we outline the possible research directions for the exploration of the structure and properties of a new material by sm-AFM.

Cyclo[18]carbon is the first sp-hybridized pure carbon ring. It was created and viewed by sm-AFM by Kaiser et al., in 2019.[18] The synthesis route and its molecular structure (and bonding features) were discussed in Bond dissociation and Molecular structure (and Interatomic bond), respectively. Stimulated by this groundbreaking work, a number of theoretical studies have been conducted to predict the structure and properties of this emerging material.[184,185] Based on these theoretical results, we provide an outlook on material investigation by sm-AFM as follows.

First, evaluate the thermal stability and thermally induced structural transformation of cyclo[18]carbon. The bonding ways of sp-hybridized carbon have long been in debate. Although the polyynic structure of cyclo[18]carbon has been demonstrated by sm-AFM at 5 K,[18] it might undergo structural transformation into a cumulenic form at an elevated temperature since the energy difference between these two forms is small.[185] In addition, heating might induce the organometallization of cyclo[18]carbon, which may greatly enhance its electrical conductivity.

Second, investigate the electronic and magnetic properties of cyclo[18]carbon. The orbital densities and charge states have been revealed by Kaiser et al.[18] As an outlook, the charge distribution can be visualized by KPFM, while the electrical conductivity can be measured by lifting the molecule with the tip and simultaneously recording the tunneling current. Furthermore, the spin and magnetic properties can be obtained using a $NiCp_2$-functionalized tip as the molecular spin sensor.

Third, measure the mechanical properties of cyclo[18]carbon. Cyclo[18]carbon has been theoretically demonstrated as an ultra-elastic molecular O-ring with tiny Young's modulus and specific tensile stiffness.[184] Thus, it is highly desirable to utilize the atomic force imposed by the sm-AFM tip to test the mechanical strength of cyclo[18]carbon. This might be conducted in the pulling, pushing, and/or lifting modes, with an emphasis on its deformation and structural recovery. Furthermore, the molecular friction can be evaluated by dragging cyclo[18]carbon with the tip.

Fourth, induce on-surface reactions via atomic manipulation. By applying a bias voltage on the tip, which is placed close to the molecule, bond dissociation and skeleton rearrangement are expected to result. On the one hand, it is desirable to observe the atomic sp-hybridized carbon chain after dissociating the bond of cyclo[18]carbon. On the other hand, atomic manipulation offers the possibility to fuse cyclo[18]carbon into larger rings. Other intriguing reactions are also highly expected.

CONCLUSIONS AND OUTLOOK

In conclusion, the booming development of sm-AFM opens the door to the atomic world, enabling us to see, manipulate, and thermally activate single molecules and even single atoms. Owing to the sharp atomic contrast, which mainly arises from the Pauli repulsion between the tip and the sample, the molecular structure can be clearly identified. The high atomic resolution also enables the visualization of interatomic bonds and adsorption geometries. Also, due to the stabilization effect of the ultralow temperature and the ultrahigh vacuum, images of the highly reactive intermediates can be captured, which directly reveal the pathway of chemical reactions and physical transitions. Moreover, sm-AFM is a powerful tool to help to unveil the composition of naturally occurring complex mixtures, such as asphaltene. Extension of the sm-AFM technique further realizes the detection of the electronic, magnetic, and chemical properties.

As well as for observing molecular structures and properties, sm-AFM is an advanced tool for single molecule/atom manipulation, on the basis of atomic force, tunneling current, or electric field. While pulling, lifting, and folding depend on the attractive interaction between the tip and the molecule/atom, pushing is achieved with the

repulsive interaction. Among these modes, lifting has received the greatest attention, with a wide range of applications, ranging from conductance measurement and friction evaluation to fabrication of single-electron field emitters and electrostatic catalysis. Also, charging, as an important manipulation approach, is capable of inducing a change in molecular conformation, aromaticity, vibronic mode, energy gap, etc. Furthermore, on-surface reactions can be realized by tip-induced manipulation, with bond dissociation and subsequent atomic rearrangement or intermolecular coupling.

Thermally activating pre-deposited single molecules is another important aspect of sm-AFM applications, mainly for on-surface production of large covalently bonded defect-free structures with repeating units. Temperature imposes kinetic control for molecular diffusion, collision, reorganization, and desorption, while the substrate serves as a catalytic template. So far, on-surface dehydrogenation, cyclodehydrogenation, dehalogenation, and organometallization have been widely investigated for synthesis of polymers and PAHs, outperforming conventional solution-based routes that are limited by molecular solubility and reactivity.

Despite the inspiring progress over the last few years, there still remains three challenges that deserve more attention in future research. First, current sm-AFM equipment with atomic resolution works under extreme conditions with a relatively long acquisition time. To stabilize the system, an ultralow temperature of ~5 K is required, and achieved by expensive liquid helium. Therefore, it is highly expected to develop high-resolution sm-AFM that operates at 77 K, or even room temperature, to reduce the cost and make the observed structures and properties closer to those in operando conditions. To realize this, the tip must be very sharp and the sample must be strongly adsorbed on the surface. Inspiringly, sub-molecular contrast has been realized at room temperature using optical interferometry with a soft Si cantilever.[38] However, the contrast is still blunt, requiring more effort into improvement of the equipment. In addition, the current acquisition time for an atomically resolved sm-AFM image is about 10 min; reduction of this time will promote the statistical analysis of molecular mixtures and the acquisition of more complex spectroscopic images, such as KPFM mapping.

Second, it is hard to accurately discriminate different elements and visualize non-planar molecules. Typically, identification of elements is based on their different van der Waals radii, while the modulated local charge density, bonding geometry, and substrate interactions significantly influence the atomic contrast. Currently, different composing elements are indicated by brighter or darker features in sm-AFM images, whereas direct evidence is lacking. The non-planarity of the molecules even makes the atomic contrast more complicated due to the different distances to the tip. In addition, the undesirable contact between the tip and the molecules can cause the contamination and even destruction of the tip. So far, some strategies have been exploited for identification of elements and non-planar molecule visualization, but more efforts are still needed, which should be coupled with the development of image databases and identification models.

Third, the underlying mechanism of on-surface reactions remains elusive. The tip-induced on-surface reaction involves bond dissociation and association, in which the former is achieved by energy transfer from the tip to the target molecule, while the latter requires not only energy provision but also certain distance and orientation of the reacting molecules. However, these aspects and the roles of the tip have not yet been investigated. Thermally induced on-surface reaction can be even more

complex, including molecular diffusion, collision, reorganization, and desorption, as mentioned above. However, current studies mainly focus on the result of on-surface reactions but ignore the process. The in-depth investigation of each step involved in thermally induced on-surface reactions is highly expected, which will help us to control the reaction orientation and rate.

Furthermore, with regard to the future, state-of-the-art sm-AFM could be incorporated with other techniques, such as STM, IR spectroscopy, Raman spectroscopy, luminescence spectroscopy, and electron paramagnetic resonance spectroscopy, to acquire more information down to the atomic scale.[122,125–127] As a most promising technology, sm-AFM has proven how magic the atomic world is, not only enabling us to see the atoms, but also, more attractively, allowing us to manipulate the atoms. We believe that, by combining the improvement of the instrumentation and model construction, more exciting discoveries are ahead.

ACKNOWLEDGMENTS

We are grateful for support from the National Science Foundation (CMMI-1661699) and the ACS Petroleum Research Fund (PRF-60329-ND10).

AUTHOR CONTRIBUTIONS

Writing – Original Draft, S.F.; Writing – Review & Editing, Y.H.H.; Supervision, Y.H.H.

REFERENCES

1. Binnig, G., Quate, C.F., and Gerber, C. (1986). Atomic force microscope. Phys. Rev. Lett. *56*, 930–933.
2. Gross, L., Mohn, F., Moll, N., Liljeroth, P., and Meyer, G. (2009). The chemical structure of a molecule resolved by atomic force microscopy. Science *325*, 1110.
3. Gross, L., Mohn, F., Moll, N., Schuler, B., Criado, A., Guitián, E., Peña, D., Gourdon, A., and Meyer, G. (2012). Bond-order discrimination by atomic force microscopy. Science *337*, 1326–1329.
4. Zhang, J., Chen, P., Yuan, B., Ji, W., Cheng, Z., and Qiu, X. (2013). Real-space identification of intermolecular bonding with atomic force microscopy. Science *342*, 611.
5. Han, Z., Czap, G., Chiang, C.-l., Xu, C., Wagner, P.J., Wei, X., Zhang, Y., Wu, R., and Ho, W. (2017). Imaging the halogen bond in self-assembled halogenbenzenes on silver. Science *358*, 206–210.
6. Emmrich, M., Huber, F., Pielmeier, F., Welker, J., Hofmann, T., Schneiderbauer, M., Meuer, D., Polesya, S., Mankovsky, S., Ködderitzsch, D., et al. (2015). Subatomic resolution force microscopy reveals internal structure and adsorption sites of small iron clusters. Science *348*, 308–311.
7. de Oteyza, D.G., Gorman, P., Chen, Y.-C., Wickenburg, S., Riss, A., Mowbray, D.J., Etkin, G., Pedramrazi, Z., Tsai, H.-Z., Rubio, A., et al. (2013). Direct imaging of covalent bond structure in single-molecule chemical reactions. Science *340*, 1434.
8. Ma, R., Cao, D., Zhu, C., Tian, Y., Peng, J., Guo, J., Chen, J., Li, X.-Z., Francisco, J.S., Zeng, X.C., et al. (2020). Atomic imaging of the edge structure and growth of a two-dimensional hexagonal ice. Nature *577*, 60–63.
9. Kawai, S., Benassi, A., Gnecco, E., Söde, H., Pawlak, R., Feng, X., Müllen, K., Passerone, D., Pignedoli, C.A., Ruffieux, P., et al. (2016). Superlubricity of graphene nanoribbons on gold surfaces. Science *351*, 957–961.
10. Esat, T., Friedrich, N., Tautz, F.S., and Temirov, R. (2018). A standing molecule as a single-electron field emitter. Nature *558*, 573–576.
11. Aragonès, A.C., Haworth, N.L., Darwish, N., Ciampi, S., Bloomfield, N.J., Wallace, G.G., Diez-Perez, I., and Coote, M.L. (2016). Electrostatic catalysis of a Diels–Alder reaction. Nature *531*, 88–91.
12. Lafferentz, L., Ample, F., Yu, H., Hecht, S., Joachim, C., and Grill, L. (2009). Conductance of a single conjugated polymer as a continuous function of its length. Science *323*, 1193–1197.
13. Peller, D., Kastner, L.Z., Buchner, T., Roelcke, C., Albrecht, F., Moll, N., Huber, R., and Repp, J. (2020). Sub-cycle atomic-scale forces coherently control a single-molecule switch. Nature *585*, 58–62.
14. Fatayer, S., Albrecht, F., Zhang, Y., Urbonas, D., Peña, D., Moll, N., and Gross, L. (2019). Molecular structure elucidation with charge-state control. Science *365*, 142–145.
15. Massee, F., Huang, Y.K., and Aprili, M. (2020). Atomic manipulation of the gap in $Bi_2Sr_2CaCu_2O_{8+x}$. Science *367*, 68–71.
16. Aragonès, A.C., Darwish, N., Ciampi, S., Sanz, F., Gooding, J.J., and Díez-Pérez, I. (2017). Single-molecule electrical contacts on silicon electrodes under ambient conditions. Nat. Comm. *8*, 15056.
17. Chen, H., Zhang, X.-L., Zhang, Y.-Y., Wang, D., Bao, D.-L., Que, Y., Xiao, W., Du, S., Ouyang, M., Pantelides, S.T., et al. (2019). Atomically precise, custom-design origami graphene nanostructures. Science *365*, 1036–1040.
18. Kaiser, K., Scriven, L.M., Schulz, F., Gawel, P., Gross, L., and Anderson, H.L. (2019). An sp-hybridized molecular carbon allotrope, cyclo [18]carbon. Science *365*, 1299.
19. Pavliček, N., Gawel, P., Kohn, D.R., Majzik, Z., Xiong, Y., Meyer, G., Anderson, H.L., and Gross, L. (2018). Polyyne formation via skeletal rearrangement induced by atomic manipulation. Nat. Chem. *10*, 853–858.
20. Pavliček, N., Schuler, B., Collazos, S., Moll, N., Pérez, D., Guitián, E., Meyer, G., Peña, D., and Gross, L. (2015). On-surface generation and imaging of arynes by atomic force microscopy. Nat. Chem. *7*, 623–628.
21. Schuler, B., Fatayer, S., Mohn, F., Moll, N., Pavliček, N., Meyer, G., Peña, D., and Gross, L. (2016). Reversible Bergman cyclization by atomic manipulation. Nat. Chem. *8*, 220–224.
22. Pavliček, N., Mistry, A., Majzik, Z., Moll, N., Meyer, G., Fox, D.J., and Gross, L. (2017). Synthesis and characterization of triangulene. Nat. Nanotechnol. *12*, 308–311.
23. Wang, S., Sun, Q., Gröning, O., Widmer, R., Pignedoli, C.A., Cai, L., Yu, X., Yuan, B., Li, C., Ju, H., et al. (2019). On-surface synthesis and characterization of individual polyacetylene chains. Nat. Chem. *11*, 924–930.
24. Cirera, B., Sánchez-Grande, A., de la Torre, B., Santos, J., Edalatmanesh, S., Rodríguez-Sánchez, E., Lauwaet, K., Mallada, B., Zbořil,

R., Miranda, R., et al. (2020). Tailoring topological order and π-conjugation to engineer quasi-metallic polymers. Nat. Nanotechnol. *15*, 437–443.

25. Cai, J., Ruffieux, P., Jaafar, R., Bieri, M., Braun, T., Blankenburg, S., Muoth, M., Seitsonen, A.P., Saleh, M., Feng, X., et al. (2010). Atomically precise bottom-up fabrication of graphene nanoribbons. Nature *466*, 470–473.

26. Ruffieux, P., Wang, S., Yang, B., Sánchez-Sánchez, C., Liu, J., Dienel, T., Talirz, L., Shinde, P., Pignedoli, C.A., Passerone, D., et al. (2016). On-surface synthesis of graphene nanoribbons with zigzag edge topology. Nature *531*, 489–492.

27. Nguyen, G.D., Tsai, H.-Z., Omrani, A.A., Marangoni, T., Wu, M., Rizzo, D.J., Rodgers, G.F., Cloke, R.R., Durr, R.A., Sakai, Y., et al. (2017). Atomically precise graphene nanoribbon heterojunctions from a single molecular precursor. Nat. Nanotechnol. *12*, 1077–1082.

28. Shekhirev, M., Zahl, P., and Sinitskii, A. (2018). Phenyl functionalization of atomically precise graphene nanoribbons for engineering inter-ribbon interactions and graphene nanopores. ACS Nano *12*, 8662–8669.

29. Talirz, L., Ruffieux, P., and Fasel, R. (2016). On-surface synthesis of atomically precise graphene nanoribbons. Adv. Mater. *28*, 6222–6231.

30. Sweetman, A., Champness, N.R., and Saywell, A. (2020). On-surface chemical reactions characterised by ultra-high resolution scanning probe microscopy. Chem. Soc. Rev. *49*, 4189–4202.

31. Gross, L., Schuler, B., Pavliček, N., Fatayer, S., Majzik, Z., Moll, N., Peña, D., and Meyer, G. (2018). Atomic force microscopy for molecular structure elucidation. Angew. Chem. Int. Ed. *57*, 3888–3908.

32. Czap, G., Wagner, P.J., Xue, F., Gu, L., Li, J., Yao, J., Wu, R., and Ho, W. (2019). Probing and imaging spin interactions with a magnetic single-molecule sensor. Science *364*, 670–673.

33. Verlhac, B., Bachellier, N., Garnier, L., Ormaza, M., Abufager, P., Robles, R., Bocquet, M.L., Ternes, M., Lorente, N., and Limot, L. (2019). Atomic-scale spin sensing with a single molecule at the apex of a scanning tunneling microscope. Science *366*, 623.

34. Hapala, P., Kichin, G., Wagner, C., Tautz, F.S., Temirov, R., and Jelínek, P. (2014). Mechanism of high-resolution STM/AFM imaging with functionalized tips. Phys. Rev. B *90*, 085421.

35. Sader, J.E., Hughes, B.D., Huber, F., and Giessibl, F.J. (2018). Interatomic force laws that evade dynamic measurement. Nat. Nanotechnol. *13*, 1088–1091.

36. Mohn, F., Schuler, B., Gross, L., and Meyer, G. (2013). Different tips for high-resolution atomic force microscopy and scanning tunneling microscopy of single molecules. Appl. Phys. Lett. *102*, 073109.

37. Mönig, H., Amirjalayer, S., Timmer, A., Hu, Z., Liu, L., Díaz Arado, O., Cnudde, M., Strassert, C.A., Ji, W., Rohlfing, M., et al. (2018). Quantitative assessment of intermolecular interactions by atomic force microscopy imaging using copper oxide tips. Nat. Nanotechnol. *13*, 371–375.

38. Iwata, K., Yamazaki, S., Mutombo, P., Hapala, P., Ondráček, M., Jelínek, P., and Sugimoto, Y. (2015). Chemical structure imaging of a single molecule by atomic force microscopy at room temperature. Nat. Comm. *6*, 7766.

39. Schuler, B., Liu, W., Tkatchenko, A., Moll, N., Meyer, G., Mistry, A., Fox, D., and Gross, L. (2013). Adsorption geometry determination of single molecules by atomic force microscopy. Phys. Rev. Lett. *111*, 106103.

40. Weymouth, A.J., Hofmann, T., and Giessibl, F.J. (2014). Quantifying molecular stiffness and interaction with lateral force microscopy. Science *343*, 1120.

41. Neu, M., Moll, N., Gross, L., Meyer, G., Giessibl, F.J., and Repp, J. (2014). Image correction for atomic force microscopy images with functionalized tips. Phys. Rev. B *89*, 205407.

42. Giessibl, F.J. (1998). High-speed force sensor for force microscopy and profilometry utilizing a quartz tuning fork. Appl. Phys. Lett. *73*, 3956–3958.

43. Giessibl, F.J. (2019). The qPlus sensor, a powerful core for the atomic force microscope. Rev. Sci. Instrum. *90*, 011101.

44. Lique, F., Willitsch, S., Ye, J., Sims, I., Bergeat, A., Vilesov, A., Lepers, M., Koch, C., Quemener, G., and Tscherbul, T. (2017). Cold Chemistry: Molecular Scattering and Reactivity Near Absolute Zero (Royal Society of Chemistry).

45. Shen, B., Zhang, Y., Komijani, Y., Nicklas, M., Borth, R., Wang, A., Chen, Y., Nie, Z., Li, R., Lu, X., et al. (2020). Strange-metal behaviour in a pure ferromagnetic Kondo lattice. Nature *579*, 51–55.

46. Martelli, V., Cai, A., Nica, E.M., Taupin, M., Prokofiev, A., Liu, C.-C., Lai, H.-H., Yu, R., Ingersent, K., Küchler, R., et al. (2019). Sequential localization of a complex electron fluid. Proc. Nat. Acad. Sci. U S A. *116*, 17701–17706.

47. Zuzak, R., Dorel, R., Kolmer, M., Szymonski, M., Godlewski, S., and Echavarren, A.M. (2018). Higher acenes by on-surface dehydrogenation: from heptacene to undecacene. Angew. Chem. Int. Ed. *57*, 10500–10505.

48. Urgel, J.I., Mishra, S., Hayashi, H., Wilhelm, J., Pignedoli, C.A., Di Giovannantonio, M., Widmer, R., Yamashita, M., Hieda, N., Ruffieux, P., et al. (2019). On-surface light-induced generation of higher acenes and elucidation of their open-shell character. Nat. Comm. *10*, 861.

49. Stetsovych, O., Švec, M., Vacek, J., Chocholoušová, J.V., Jančařík, A., Rybáček, J., Kosmider, K., Stará, I.G., Jelínek, P., and Starý, I. (2017). From helical to planar chirality by on-surface chemistry. Nat. Chem. *9*, 213–218.

50. Su, J., Telychko, M., Hu, P., Macam, G., Mutombo, P., Zhang, H., Bao, Y., Cheng, F., Huang, Z.-Q., Qiu, Z., et al. (2019). Atomically precise bottom-up synthesis of π-extended [5]triangulene. Sci. Adv. *5*, eaav7717.

51. Liu, M., Li, S., Zhou, J., Zha, Z., Pan, J., Li, X., Zhang, J., Liu, Z., Li, Y., and Qiu, X. (2018). High-yield formation of graphdiyne macrocycles through on-surface assembling and coupling reaction. ACS Nano *12*, 12612–12618.

52. Yu, X., Li, X., Lin, H., Liu, M., Cai, L., Qiu, X., Yang, D., Fan, X., Qiu, X., and Xu, W. (2020). Bond-scission-induced structural transformation from cumulene to diyne moiety and formation of semiconducting organometallic polyyne. J. Am. Chem. Soc. *142*, 8085–8089.

53. Scriven, L.M., Kaiser, K., Schulz, F., Sterling, A.J., Woltering, S.L., Gawel, P., Christensen, K.E., Anderson, H.L., and Gross, L. (2020). Synthesis of cyclo[18]carbon via debromination of $C_{18}Br_6$. J. Am. Chem. Soc. *142*, 12921–12924.

54. Moreno, C., Stetsovych, O., Shimizu, T.K., and Custance, O. (2015). Imaging three-dimensional surface objects with submolecular resolution by atomic force microscopy. Nano Lett. *15*, 2257–2262.

55. Liu, X., and Hersam, M.C. (2019). Borophene-graphene heterostructures. Sci. Adv. *5*, eaax6444.

56. Wu, R., Drozdov, I.K., Eltinge, S., Zahl, P., Ismail-Beigi, S., Božović, I., and Gozar, A. (2019). Large-area single-crystal sheets of borophene on Cu(111) surfaces. Nat. Nanotechnol. *14*, 44–49.

57. Schwarz, M., Riss, A., Garnica, M., Ducke, J., Deimel, P.S., Duncan, D.A., Thakur, P.K., Lee, T.-L., Seitsonen, A.P., Barth, J.V., et al. (2017). Corrugation in the weakly interacting hexagonal-BN/Cu(111) system: structure determination by combining noncontact atomic force microscopy and X-ray standing waves. ACS Nano *11*, 9151–9161.

58. Barja, S., Refaely-Abramson, S., Schuler, B., Qiu, D.Y., Pulkin, A., Wickenburg, S., Ryu, H., Ugeda, M.M., Kastl, C., Chen, C., et al. (2019). Identifying substitutional oxygen as a prolific point defect in monolayer transition metal dichalcogenides. Nat. Comm. *10*, 3382.

59. Zuzak, R., Pozo, I., Engelund, M., Garcia-Lekue, A., Vilas-Varela, M., Alonso, J.M., Szymonski, M., Guitián, E., Pérez, D., Godlewski, S., et al. (2019). Synthesis and reactivity of a trigonal porous nanographene on a gold surface. Chem. Sci. *10*, 10143–10148.

60. Xu, K., Urgel, J.I., Eimre, K., Di Giovannantonio, M., Keerthi, A., Komber, H., Wang, S., Narita, A., Berger, R., Ruffieux, P., et al. (2019). On-surface synthesis of a nonplanar porous nanographene. J. Am. Chem. Soc. *141*, 7726–7730.

61. Mishra, S., Beyer, D., Berger, R., Liu, J., Gröning, O., Urgel, J.I., Müllen, K., Ruffieux, P., Feng, X., and Fasel, R. (2020). Topological defect-induced magnetism in a nanographene. J. Am. Chem. Soc. *142*, 1147–1152.

62. Kawai, S., Nakatsuka, S., Hatakeyama, T., Pawlak, R., Meier, T., Tracey, J., Meyer, E., and Foster, A.S. (2018). Multiple heteroatom

substitution to graphene nanoribbon. Sci. Adv. *4*, eaar7181.

63. de la Torre, B., Švec, M., Hapala, P., Redondo, J., Krejčí, O., Lo, R., Manna, D., Sarmah, A., Nachtigallová, D., Tuček, J., et al. (2018). Non-covalent control of spin-state in metal-organic complex by positioning on N-doped graphene. Nat. Comm. *9*, 2831.

64. Durr, R.A., Haberer, D., Lee, Y.-L., Blackwell, R., Kalayjian, A.M., Marangoni, T., Ihm, J., Louie, S.G., and Fischer, F.R. (2018). Orbitally matched edge-doping in graphene nanoribbons. J. Am. Chem. Soc. *140*, 807–813.

65. Liu, M., Liu, M., Zha, Z., Pan, J., Qiu, X., Li, T., Wang, J., Zheng, Y., and Zhong, D. (2018). Thermally induced transformation of nonhexagonal carbon rings in graphene-like nanoribbons. J. Phys. Chem. C *122*, 9586–9592.

66. Dienel, T., Kawai, S., Söde, H., Feng, X., Müllen, K., Ruffieux, P., Fasel, R., and Gröning, O. (2015). Resolving atomic connectivity in graphene nanostructure junctions. Nano Lett. *15*, 5185–5190.

67. Huang, C., Li, Y., Wang, N., Xue, Y., Zuo, Z., Liu, H., and Li, Y. (2018). Progress in research into 2D graphdiyne-based materials. Chem. Rev. *118*, 7744–7803.

68. Peng, J., Guo, J., Hapala, P., Cao, D., Ma, R., Cheng, B., Xu, L., Ondráček, M., Jelínek, P., Wang, E., et al. (2018). Weakly perturbative imaging of interfacial water with submolecular resolution by atomic force microscopy. Nat. Comm. *9*, 122.

69. Shiotari, A., Sugimoto, Y., and Kamio, H. (2019). Characterization of two- and one-dimensional water networks on Ni(111) via atomic force microscopy. Phys. Rev. Mater. *3*, 093001.

70. Shiotari, A., and Sugimoto, Y. (2017). Ultrahigh-resolution imaging of water networks by atomic force microscopy. Nat. Comm. *8*, 14313.

71. Gross, L., Mohn, F., Moll, N., Meyer, G., Ebel, R., Abdel-Mageed, W.M., and Jaspars, M. (2010). Organic structure determination using atomic-resolution scanning probe microscopy. Nat. Chem. *2*, 821–825.

72. Hanssen, K.Ø., Schuler, B., Williams, A.J., Demissie, T.B., Hansen, E., Andersen, J.H., Svenson, J., Blinov, K., Repisky, M., Mohn, F., et al. (2012). A combined atomic force microscopy and computational approach for the structural elucidation of breitfussin A and B: highly modified halogenated dipeptides from *Thuiaria breitfussi*. Angew. Chem. Int. Ed. *51*, 12238–12241.

73. Biel, B., Blase, X., Triozon, F., and Roche, S. (2009). Anomalous doping effects on charge transport in graphene nanoribbons. Phys. Rev. Lett. *102*, 096803.

74. Schulz, F., Ritala, J., Krejčí, O., Seitsonen, A.P., Foster, A.S., and Liljeroth, P. (2018). Elemental identification by combining atomic force microscopy and Kelvin probe force microscopy. ACS Nano *12*, 5274–5283.

75. Zahl, P., and Zhang, Y. (2019). Guide for atomic force microscopy image analysis to discriminate heteroatoms in aromatic molecules. Energy & Fuels *33*, 4775–4780.

76. Welker, J., and Giessibl, F.J. (2012). Revealing the angular symmetry of chemical bonds by atomic force microscopy. Science *336*, 444.

77. Fang, S., and Hu, Y.H. (2019). Creating and seeing the first pure carbon ring. Matter *1*, 1116–1118.

78. Urgel, J.I., Di Giovannantonio, M., Eimre, K., Lohr, T.G., Liu, J., Mishra, S., Sun, Q., Kinikar, A., Widmer, R., and Stolz, S. (2020). On-surface synthesis of cumulene-containing polymers via two-step dehalogenative homocoupling of dibromomethylene-functionalized tribenzoazulene. Angew. Chem. Int. Ed. *59*, 13281–13287.

79. He, Y., Garnica, M., Bischoff, F., Ducke, J., Bocquet, M.-L., Batzill, M., Auwärter, W., and Barth, J.V. (2017). Fusing tetrapyrroles to graphene edges by surface-assisted covalent coupling. Nat. Chem. *9*, 33–38.

80. Majzik, Z., Pavliček, N., Vilas-Varela, M., Pérez, D., Moll, N., Guitián, E., Meyer, G., Peña, D., and Gross, L. (2018). Studying an antiaromatic polycyclic hydrocarbon adsorbed on different surfaces. Nat. Comm. *9*, 1198.

81. Sánchez-Grande, A., de la Torre, B., Santos, J., Cirera, B., Lauwaet, K., Chutora, T., Edalatmanesh, S., Mutombo, P., Rosen, J., Zbořil, R., et al. (2019). On-surface synthesis of ethynylene-bridged anthracene polymers. Angew. Chem. Int. Ed. *58*, 6559–6563.

82. Kawai, S., Krejčí, O., Foster, A.S., Pawlak, R., Xu, F., Peng, L., Orita, A., and Meyer, E. (2018). Diacetylene linked anthracene oligomers synthesized by one-shot homocoupling of trimethylsilyl on Cu(111). ACS Nano *12*, 8791–8797.

83. Albrecht, F., Neu, M., Quest, C., Swart, I., and Repp, J. (2013). Formation and characterization of a molecule–metal–molecule bridge in real space. J. Am. Chem. Soc. *135*, 9200–9203.

84. Sweetman, A.M., Jarvis, S.P., Sang, H., Lekkas, I., Rahe, P., Wang, Y., Wang, J., Champness, N.R., Kantorovich, L., and Moriarty, P. (2014). Mapping the force field of a hydrogen-bonded assembly. Nat. Comm. *5*, 3931.

85. Cirera, B., de la Torre, B., Moreno, D., Ondráček, M., Zbořil, R., Miranda, R., Jelínek, P., and Écija, D. (2019). On-surface synthesis of gold porphyrin derivatives via a cascade of chemical interactions: planarization, self-metalation, and intermolecular coupling. Chem. Mater. *31*, 3248–3256.

86. Kawai, S., Nishiuchi, T., Kodama, T., Spijker, P., Pawlak, R., Meier, T., Tracey, J., Kubo, T., Meyer, E., and Foster, A.S. (2017). Direct quantitative measurement of the C=O•••H–C bond by atomic force microscopy. Sci. Adv. *3*, e1603258.

87. Weymouth, A.J., Riegel, E., Gretz, O., and Giessibl, F.J. (2020). Strumming a single chemical bond. Phys. Rev. Lett. *124*, 196101.

88. Yang, S., Li, S., Filimonov, S.N., Fuentes-Cabrera, M., and Liu, W. (2018). Principles of design for substrate-supported molecular switches based on physisorbed and chemisorbed states. ACS Appl. Mater. Inter. *10*, 26772–26780.

89. Ebeling, D., Zhong, Q., Schlöder, T., Tschakert, J., Henkel, P., Ahles, S., Chi, L., Mollenhauer, D., Wegner, H.A., and Schirmeisen, A. (2019). Adsorption structure of mono- and diradicals on a Cu(111) surface: chemoselective dehalogenation of 4-bromo-3″-iodo-p-terphenyl. ACS Nano *13*, 324–336.

90. Michnowicz, T., Borca, B., Pétuya, R., Schendel, V., Pristl, M., Pentegov, I., Kraft, U., Klauk, H., Wahl, P., Mutombo, P., et al. (2020). Controlling single molecule conductance by a locally induced chemical reaction on individual thiophene units. Angew. Chem. Int. Ed. *59*, 6207–6212.

91. Zhong, Q., Ebeling, D., Tschakert, J., Gao, Y., Bao, D., Du, S., Li, C., Chi, L., and Schirmeisen, A. (2018). Symmetry breakdown of 4,4″-diamino-p-terphenyl on a Cu(111) surface by lattice mismatch. Nat. Comm. *9*, 3277.

92. Ebeling, D., Šekutor, M., Stiefermann, M., Tschakert, J., Dahl, J.E.P., Carlson, R.M.K., Schirmeisen, A., and Schreiner, P.R. (2018). Assigning the absolute configuration of single aliphatic molecules by visual inspection. Nat. Comm. *9*, 2420.

93. Huber, F., Berwanger, J., Polesya, S., Mankovsky, S., Ebert, H., and Giessibl, F.J. (2019). Chemical bond formation showing a transition from physisorption to chemisorption. Science *366*, 235.

94. Sokolović, I., Reticcioli, M., Čalkovský, M., Wagner, M., Schmid, M., Franchini, C., Diebold, U., and Setvín, M. (2020). Resolving the adsorption of molecular O_2 on the rutile TiO_2(110) surface by noncontact atomic force microscopy. Proc. Nat. Acad. Sci. U S A. *117*, 14827.

95. Meier, T., Pawlak, R., Kawai, S., Geng, Y., Liu, X., Decurtins, S., Hapala, P., Baratoff, A., Liu, S.-X., Jelínek, P., et al. (2017). Donor–acceptor properties of a single-molecule altered by on-surface complex formation. ACS Nano *11*, 8413–8420.

96. Ebeling, D., Šekutor, M., Stiefermann, M., Tschakert, J., Dahl, J.E.P., Carlson, R.M.K., Schirmeisen, A., and Schreiner, P.R. (2017). London dispersion directs on-surface self-assembly of [121]tetramantane molecules. ACS Nano *11*, 9459–9466.

97. Song, S., Guo, N., Li, X., Li, G., Haketa, Y., Telychko, M., Su, J., Lyu, P., Qiu, Z., Fang, H., et al. (2020). Real-space imaging of a single-molecule monoradical reaction. J. Am. Chem. Soc. *142*, 13550–13557.

98. Berwanger, J., Polesya, S., Mankovsky, S., Ebert, H., and Giessibl, F.J. (2020). Atomically resolved chemical reactivity of small Fe clusters. Phys. Rev. Lett. *124*, 096001.

99. Martin-Jimenez, D., Ahles, S., Mollenhauer, D., Wegner, H.A., Schirmeisen, A., and Ebeling, D. (2019). Bond-level imaging of the 3D conformation of adsorbed organic molecules using atomic force microscopy with simultaneous tunneling feedback. Phys. Rev. Lett. *122*, 196101.

100. Zint, S., Ebeling, D., Schlöder, T., Ahles, S., Mollenhauer, D., Wegner, H.A., and Schirmeisen, A. (2017). Imaging successive

intermediate states of the on-surface Ullmann reaction on Cu(111): role of the metal coordination. ACS Nano *11*, 4183–4190.

101. Albrecht, F., Bischoff, F., Auwärter, W., Barth, J.V., and Repp, J. (2016). Direct identification and determination of conformational response in adsorbed individual nonplanar molecular species using noncontact atomic force microscopy. Nano Lett. *16*, 7703–7709.

102. Alldritt, B., Hapala, P., Oinonen, N., Urtev, F., Krejci, O., Federici Canova, F., Kannala, J., Schulz, F., Liljeroth, P., and Foster, A.S. (2020). Automated structure discovery in atomic force microscopy. Sci. Adv. *6*, eaay6913.

103. Telychko, M., Su, J., Gallardo, A., Gu, Y., Mendieta-Moreno, J.I., Qi, D., Tadich, A., Song, S., Lyu, P., Qiu, Z., et al. (2019). Strain-induced isomerization in one-dimensional metal–organic chains. Angew. Chem. Int. Ed. *58*, 18591–18597.

104. Riss, A., Paz, A.P., Wickenburg, S., Tsai, H.-Z., De Oteyza, D.G., Bradley, A.J., Ugeda, M.M., Gorman, P., Jung, H.S., Crommie, M.F., et al. (2016). Imaging single-molecule reaction intermediates stabilized by surface dissipation and entropy. Nat. Chem. *8*, 678–683.

105. Schuler, B., Meyer, G., Peña, D., Mullins, O.C., and Gross, L. (2015). Unraveling the molecular structures of asphaltenes by atomic force microscopy. J. Am. Chem. Soc. *137*, 9870–9876.

106. Chen, P., Metz, J.N., Mennito, A.S., Merchant, S., Smith, S.E., Siskin, M., Rucker, S.P., Dankworth, D.C., Kushnerick, J.D., Yao, N., et al. (2020). Petroleum pitch: exploring a 50-year structure puzzle with real-space molecular imaging. Carbon *161*, 456–465.

107. Fatayer, S., Poddar, N.B., Quiroga, S., Schulz, F., Schuler, B., Kalpathy, S.V., Meyer, G., Pérez, D., Guitián, E., Peña, D., et al. (2018). Atomic force microscopy identifying fuel pyrolysis products and directing the synthesis of analytical standards. J. Am. Chem. Soc. *140*, 8156–8161.

108. Czap, G., Wagner, P.J., Li, J., Xue, F., Yao, J., Wu, R., and Ho, W. (2019). Detection of spin-vibration states in single magnetic molecules. Phys. Rev. Lett. *123*, 106803.

109. Yang, K., Paul, W., Phark, S.-H., Willke, P., Bae, Y., Choi, T., Esat, T., Ardavan, A., Heinrich, A.J., and Lutz, C.P. (2019). Coherent spin manipulation of individual atoms on a surface. Science *366*, 509–512.

110. Garnier, L., Verlhac, B., Abufager, P., Lorente, N., Ormaza, M., and Limot, L. (2020). The Kondo effect of a molecular tip as a magnetic sensor. Nano Lett. *20*, 8193–8199.

111. Li, X., Zhu, L., Li, B., Li, J., Gao, P., Yang, L., Zhao, A., Luo, Y., Hou, J., Zheng, X., et al. (2020). Molecular molds for regularizing Kondo states at atom/metal interfaces. Nat. Comm. *11*, 2566.

112. Steurer, W., Fatayer, S., Gross, L., and Meyer, G. (2015). Probe-based measurement of lateral single-electron transfer between individual molecules. Nat. Comm. *6*, 8353.

113. Patera, L.L., Queck, F., Scheuerer, P., and Repp, J. (2019). Mapping orbital changes upon electron transfer with tunnelling microscopy on insulators. Nature *566*, 245–248.

114. Pavliček, N., and Gross, L. (2017). Generation, manipulation and characterization of molecules by atomic force microscopy. Nat. Rev. Chem. *1*, 0005.

115. Schuler, B., Liu, S.-X., Geng, Y., Decurtins, S., Meyer, G., and Gross, L. (2014). Contrast formation in Kelvin probe force microscopy of single π-conjugated molecules. Nano Lett. *14*, 3342–3346.

116. Barth, C., Foster, A.S., Henry, C.R., and Shluger, A.L. (2011). Recent trends in surface characterization and chemistry with high-resolution scanning force methods. Adv. Mater. *23*, 477–501.

117. Ellner, M., Pavliček, N., Pou, P., Schuler, B., Moll, N., Meyer, G., Gross, L., and Peréz, R. (2016). The electric field of CO tips and its relevance for atomic force microscopy. Nano Lett. *16*, 1974–1980.

118. Palacios-Lidón, E., Henry, C.R., and Barth, C. (2014). Kelvin probe force microscopy in surface chemistry: reactivity of Pd nanoparticles on highly oriented pirolytic graphite. ACS Catal. *4*, 1838–1844.

119. Porkovich, A., Ziadi, Z., Kumar, P., Kioseoglou, J., Jian, N., Weng, L., Steinhauer, S., Vernieres, J., Grammatikopoulos, P., and Sowwan, M. (2019). In situ observation of metal to metal oxide progression: a study of charge transfer phenomenon at Ru–CuO interfaces. ACS Nano *13*, 12425–12437.

120. Tao, L., Qiao, M., Jin, R., Li, Y., Xiao, Z., Wang, Y., Zhang, N., Xie, C., He, Q., Jiang, D., et al. (2019). Bridging the surface charge and catalytic activity of a defective carbon electrocatalyst. Angew. Chem. Int. Ed. *58*, 1019–1024.

121. Wagner, C., Green, M.F.B., Maiworm, M., Leinen, P., Esat, T., Ferri, N., Friedrich, N., Findeisen, R., Tkatchenko, A., Temirov, R., et al. (2019). Quantitative imaging of electric surface potentials with single-atom sensitivity. Nat. Mater. *18*, 853–859.

122. Lee, J., Tallarida, N., Chen, X., Jensen, L., and Apkarian, V.A. (2018). Microscopy with a single-molecule scanning electrometer. Sci. Adv. *4*, eaat5472.

123. Liljeroth, P., Repp, J., and Meyer, G. (2007). Current-induced hydrogen tautomerization and conductance switching of naphthalocyanine molecules. Science *317*, 1203.

124. Patera, L.L., Sokolov, S., Low, J.Z., Campos, L.M., Venkataraman, L., and Repp, J. (2019). Resolving the unpaired-electron orbital distribution in a stable organic radical by Kondo resonance mapping. Angew. Chem. Int. Ed. *58*, 11063–11067.

125. Dazzi, A., and Prater, C.B. (2017). AFM-IR: technology and applications in nanoscale infrared spectroscopy and chemical imaging. Chem. Rev. *117*, 5146–5173.

126. Zhang, Y., Luo, Y., Zhang, Y., Yu, Y.-J., Kuang, Y.-M., Zhang, L., Meng, Q.-S., Luo, Y., Yang, J.-L., Dong, Z.-C., et al. (2016). Visualizing coherent intermolecular dipole–dipole coupling in real space. Nature *531*, 623–627.

127. Zhang, R., Zhang, Y., Dong, Z.C., Jiang, S., Zhang, C., Chen, L.G., Zhang, L., Liao, Y., Aizpurua, J., Luo, Y., et al. (2013). Chemical mapping of a single molecule by plasmon-enhanced Raman scattering. Nature *498*, 82–86.

128. Pozzi, E.A., Goubert, G., Chiang, N., Jiang, N., Chapman, C.T., McAnally, M.O., Henry, A.-I., Seideman, T., Schatz, G.C., Hersam, M.C., et al. (2017). Ultrahigh-vacuum tip-enhanced Raman spectroscopy. Chem. Rev. *117*, 4961–4982.

129. Eigler, D.M., and Schweizer, E.K. (1990). Positioning single atoms with a scanning tunnelling microscope. Nature *344*, 524–526.

130. Bartels, L., Meyer, G., and Rieder, K.H. (1997). Basic steps of lateral manipulation of single atoms and diatomic clusters with a scanning tunneling microscope tip. Phys. Rev. Lett. *79*, 697–700.

131. Willke, P., Bae, Y., Yang, K., Lado, J.L., Ferrón, A., Choi, T., Ardavan, A., Fernández-Rossier, J., Heinrich, A.J., and Lutz, C.P. (2018). Hyperfine interaction of individual atoms on a surface. Science *362*, 336–339.

132. Ternes, M., Lutz, C.P., Hirjibehedin, C.F., Giessibl, F.J., and Heinrich, A.J. (2008). The force needed to move an atom on a surface. Science *319*, 1066.

133. Naitoh, Y., Turanský, R., Brndiar, J., Li, Y.J., Štich, I., and Sugawara, Y. (2017). Subatomic-scale force vector mapping above a Ge(001) dimer using bimodal atomic force microscopy. Nat. Phys. *13*, 663–667.

134. Emmrich, M., Schneiderbauer, M., Huber, F., Weymouth, A.J., Okabayashi, N., and Giessibl, F.J. (2015). Force field analysis suggests a lowering of diffusion barriers in atomic manipulation due to presence of STM tip. Phys. Rev. Lett. *114*, 146101.

135. Kaku, S., and Yoshino, J. (2020). Temperature-dependent tip-induced motion of Ga adatom on GaAs (110) surface. Small *16*, 2002296.

136. Peng, J., Cao, D., He, Z., Guo, J., Hapala, P., Ma, R., Cheng, B., Chen, J., Xie, W.J., Li, X.-Z., et al. (2018). The effect of hydration number on the interfacial transport of sodium ions. Nature *557*, 701–705.

137. Shiotari, A., Odani, T., and Sugimoto, Y. (2018). Torque-induced change in configuration of a single NO molecule on Cu(110). Phys. Rev. Lett. *121*, 116101.

138. Li, C., Wang, Z., Lu, Y., Liu, X., and Wang, L. (2017). Conformation-based signal transfer and processing at the single-molecule level. Nat. Nanotechnol. *12*, 1071–1076.

139. Ladenthin, J.N., Frederiksen, T., Persson, M., Sharp, J.C., Gawinkowski, S., Waluk, J., and Kumagai, T. (2016). Force-induced tautomerization in a single molecule. Nat. Chem. *8*, 935–940.

140. Wagner, C., Fournier, N., Ruiz, V.G., Li, C., Müllen, K., Rohlfing, M., Tkatchenko, A., Temirov, R., and Tautz, F.S. (2014). Non-additivity of molecule-surface van der Waals

potentials from force measurements. Nat. Comm. *5*, 5568.

141. Clair, S., and de Oteyza, D.G. (2019). Controlling a chemical coupling reaction on a surface: tools and strategies for on-surface synthesis. Chem. Rev. *119*, 4717–4776.

142. Bamidele, J., Lee, S.H., Kinoshita, Y., Turanský, R., Naitoh, Y., Li, Y.J., Sugawara, Y., Štich, I., and Kantorovich, L. (2014). Vertical atomic manipulation with dynamic atomic-force microscopy without tip change via a multi-step mechanism. Nat. Comm. *5*, 4476.

143. Nacci, C., Ample, F., Bleger, D., Hecht, S., Joachim, C., and Grill, L. (2015). Conductance of a single flexible molecular wire composed of alternating donor and acceptor units. Nat. Comm. *6*, 7397.

144. Kawai, S., Koch, M., Gnecco, E., Sadeghi, A., Pawlak, R., Glatzel, T., Schwarz, J., Goedecker, S., Hecht, S., Baratoff, A., et al. (2014). Quantifying the atomic-level mechanics of single long physisorbed molecular chains. Proc. Nat. Acad. Sci. *111*, 3968–3972.

145. Fournier, N., Wagner, C., Weiss, C., Temirov, R., and Tautz, F.S. (2011). Force-controlled lifting of molecular wires. Phys. Rev. B *84*, 035435.

146. Borca, B., Michnowicz, T., Pétuya, R., Pristl, M., Schendel, V., Pentegov, I., Kraft, U., Klauk, H., Wahl, P., Gutzler, R., et al. (2017). Electric-field-driven direct desulfurization. ACS Nano *11*, 4703–4709.

147. Li, H.B., Tebikachew, B.E., Wiberg, C., Moth-Poulsen, K., and Hihath, J. (2020). A memristive element based on an electrically controlled single-molecule reaction. Angew. Chem. Int. Ed. *59*, 11641–11646.

148. Schendel, V., Borca, B., Pentegov, I., Michnowicz, T., Kraft, U., Klauk, H., Wahl, P., Schlickum, U., and Kern, K. (2016). Remotely controlled isomer selective molecular switching. Nano Lett. *16*, 93–97.

149. Adachi, Y., Wen, H.F., Zhang, Q., Miyazaki, M., Sugawara, Y., Sang, H., Brndiar, J., Kantorovich, L., Štich, I., and Li, Y.J. (2019). Tip-induced control of charge and molecular bonding of oxygen atoms on the rutile TiO_2(110) surface with atomic force microscopy. ACS Nano *13*, 6917–6924.

150. Kocić, N., Weiderer, P., Keller, S., Decurtins, S., Liu, S.X., and Repp, J. (2015). Periodic charging of individual molecules coupled to the motion of an atomic force microscopy tip. Nano Lett. *15*, 4406–4411.

151. Wickenburg, S., Lu, J., Lischner, J., Tsai, H.-Z., Omrani, A.A., Riss, A., Karrasch, C., Bradley, A., Jung, H.S., Khajeh, R., et al. (2016). Tuning charge and correlation effects for a single molecule on a graphene device. Nat. Comm. *7*, 13553.

152. Pavliček, N., Majzik, Z., Collazos, S., Meyer, G., Pérez, D., Guitián, E., Peña, D., and Gross, L. (2017). Generation and characterization of a meta-aryne on Cu and NaCl surfaces. ACS Nano *11*, 10768–10773.

153. Schulz, F., García, F., Kaiser, K., Pérez, D., Guitián, E., Gross, L., and Peña, D. (2019). Exploring a route to cyclic acenes by on-surface synthesis. Angew. Chem. Int. Ed. *58*, 9038–9042.

154. Albrecht, F., Rey, D., Fatayer, S., Pérez, D., Peña, D., and Gross, L. (2020). Intramolecular coupling of terminal alkynes by atom manipulation. Angew. Chem. Int. Ed. *59*, 22989–22993.

155. Di Giovannantonio, M., Deniz, O., Urgel, J.I., Widmer, R., Dienel, T., Stolz, S., Sánchez-Sánchez, C., Muntwiler, M., Dumslaff, T., Berger, R., et al. (2018). On-surface growth dynamics of graphene nanoribbons: the role of halogen functionalization. ACS Nano *12*, 74–81.

156. Fan, Q., Martin-Jimenez, D., Ebeling, D., Krug, C.K., Brechmann, L., Kohlmeyer, C., Hilt, G., Hieringer, W., Schirmeisen, A., and Gottfried, J.M. (2019). Nanoribbons with nonalternant topology from fusion of polyazulene: carbon allotropes beyond graphene. J. Am. Chem. Soc. *141*, 17713–17720.

157. Sun, Q., Yu, X., Bao, M., Liu, M., Pan, J., Zha, Z., Cai, L., Ma, H., Yuan, C., Qiu, X., et al. (2018). Direct formation of C–C triple-bonded structural motifs by on-surface dehalogenative homocouplings of tribromomethyl-substituted arenes. Angew. Chem. Int. Ed. *57*, 4035–4038.

158. Sánchez-Sánchez, C., Dienel, T., Nicolaï, A., Kharche, N., Liang, L., Daniels, C., Meunier, V., Liu, J., Feng, X., Müllen, K., et al. (2019). On-surface synthesis and characterization of acene-based nanoribbons incorporating four-membered rings. Chem. Eur. J. *25*, 12074–12082.

159. Liu, J., Chen, Q., Cai, K., Li, J., Li, Y., Yang, X., Zhang, Y., Wang, Y., Tang, H., Zhao, D., et al. (2019). Stepwise on-surface dissymmetric reaction to construct binodal organometallic network. Nat. Comm. *10*, 2545.

160. Blanksby, S.J., and Ellison, G.B. (2003). Bond dissociation energies of organic molecules. Acc. Chem. Res. *36*, 255–263.

161. Kawai, S., Krejčí, O., Nishiuchi, T., Sahara, K., Kodama, T., Pawlak, R., Meyer, E., Kubo, T., and Foster, A.S. (2020). Three-dimensional graphene nanoribbons as a framework for molecular assembly and local probe chemistry. Sci. Adv. *6*, eaay8913.

162. Kaiser, K., Gross, L., and Schulz, F. (2019). A single-molecule chemical reaction studied by high-resolution atomic force microscopy and scanning tunneling microscopy induced light emission. ACS Nano *13*, 6947–6954.

163. Jiang, Y., Huan, Q., Fabris, L., Bazan, G.C., and Ho, W. (2013). Submolecular control, spectroscopy and imaging of bond-selective chemistry in single functionalized molecules. Nat. Chem. *5*, 36–41.

164. Shiotari, A., Nakae, T., Iwata, K., Mori, S., Okujima, T., Uno, H., Sakaguchi, H., and Sugimoto, Y. (2017). Strain-induced skeletal rearrangement of a polycyclic aromatic hydrocarbon on a copper surface. Nat. Comm. *8*, 16089.

165. Bischoff, F., He, Y., Riss, A., Seufert, K., Auwärter, W., and Barth, J.V. (2018). Exploration of interfacial porphine coupling schemes and hybrid systems by bond-resolved scanning probe microscopy. Angew. Chem. Int. Ed. *57*, 16030–16035.

166. Sánchez-Sánchez, C., Martínez, J.I., Ruiz del Arbol, N., Ruffieux, P., Fasel, R., López, M.F., de Andres, P.L., and Martín-Gago, J.Á. (2019). On-surface hydrogen-induced covalent coupling of polycyclic aromatic hydrocarbons via a superhydrogenated intermediate. J. Am. Chem. Soc. *141*, 3550–3557.

167. Li, J., Merino-Díez, N., Carbonell-Sanromà, E., Vilas-Varela, M., de Oteyza, D.G., Peña, D., Corso, M., and Pascual, J.I. (2018). Survival of spin state in magnetic porphyrins contacted by graphene nanoribbons. Sci. Adv. *4*, eaaq0582.

168. Pinardi, A.L., Otero-Irurueta, G., Palacio, I., Martinez, J.I., Sanchez-Sanchez, C., Tello, M., Rogero, C., Cossaro, A., Preobrajenski, A., Gómez-Lor, B., et al. (2013). Tailored formation of N-doped nanoarchitectures by diffusion-controlled on-surface (cyclo) dehydrogenation of heteroaromatics. ACS Nano *7*, 3676–3684.

169. Kawai, S., Haapasilta, V., Lindner, B.D., Tahara, K., Spijker, P., Buitendijk, J.A., Pawlak, R., Meier, T., Tobe, Y., Foster, A.S., et al. (2016). Thermal control of sequential on-surface transformation of a hydrocarbon molecule on a copper surface. Nat. Comm. *7*, 12711.

170. Blankenburg, S., Cai, J., Ruffieux, P., Jaafar, R., Passerone, D., Feng, X., Müllen, K., Fasel, R., and Pignedoli, C.A. (2012). Intraribbon heterojunction formation in ultranarrow graphene nanoribbons. ACS Nano *6*, 2020–2025.

171. Stolz, S., Di Giovannantonio, M., Urgel, J.I., Sun, Q., Kinikar, A., Borin Barin, G., Bommert, M., Fasel, R., and Widmer, R. (2020). Reversible dehalogenation in on-surface aryl-aryl coupling. Angew. Chem. Int. Ed. *59*, 14106–14110.

172. Bronner, C., Björk, J., and Tegeder, P. (2015). Tracking and removing Br during the on-surface synthesis of a graphene nanoribbon. J. Phys. Chem. C *119*, 486–493.

173. Urgel, J.I., Hayashi, H., Di Giovannantonio, M., Pignedoli, C.A., Mishra, S., Deniz, O., Yamashita, M., Dienel, T., Ruffieux, P., Yamada, H., et al. (2017). On-surface synthesis of heptacene organometallic complexes. J. Am. Chem. Soc. *139*, 11658–11661.

174. Sun, Q., Cai, L., Wang, S., Widmer, R., Ju, H., Zhu, J., Li, L., He, Y., Ruffieux, P., Fasel, R., et al. (2016). Bottom-up synthesis of metalated carbyne. J. Am. Chem. Soc. *138*, 1106–1109.

175. Hellerstedt, J., Cahlík, A., Stetsovych, O., Švec, M., Shimizu, T.K., Mutombo, P., Klívar, J., Stará, I.G., Jelínek, P., and Starý, I. (2019). Aromatic azide transformation on the Ag(111) surface studied by scanning probe microscopy. Angew. Chem. Int. Ed. *58*, 2266–2271.

176. Krüger, J., García, F., Eisenhut, F., Skidin, D., Alonso, J.M., Guitián, E., Pérez, D., Cuniberti, G., Moresco, F., and Peña, D. (2017). Decacene: on-surface generation. Angew. Chem. Int. Ed. *56*, 11945–11948.

177. Li, Q., Gao, J., Li, Y., Fuentes-Cabrera, M., Liu, M., Qiu, X., Lin, H., Chi, L., and Pan, M. (2018). Self-assembly directed one-step synthesis of [4]

radialene on Cu(100) surfaces. Nat. Comm. *9*, 3113.

178. Kim, M., and Chelikowsky, J.R. (2015). CO tip functionalization in subatomic resolution atomic force microscopy. Appl. Phys. Lett. *107*, 163109.

179. Lee, A.J., Sakai, Y., Kim, M., and Chelikowsky, J.R. (2016). Repulsive tip tilting as the dominant mechanism for hydrogen bond-like features in atomic force microscopy imaging. Appl. Phys. Lett. *108*, 193102.

180. Guo, C.-S., Xin, X., Van Hove, M.A., Ren, X., and Zhao, Y. (2015). Origin of the contrast interpreted as intermolecular and intramolecular bonds in atomic force microscopy images. J. Phys. Chem. C *119*, 14195–14200.

181. Chan, T.L., Wang, C.Z., Ho, K.M., and Chelikowsky, J.R. (2009). Efficient first-principles simulation of noncontact atomic force microscopy for structural analysis. Phys. Rev. Lett. *102*, 176101.

182. Ellner, M., Pou, P., and Pérez, R. (2019). Molecular identification, bond order discrimination, and apparent intermolecular features in atomic force microscopy studied with a charge density based method. ACS Nano *13*, 786–795.

183. Wesolowski, T.A., Shedge, S., and Zhou, X. (2015). Frozen-density embedding strategy for multilevel simulations of electronic structure. Chem. Rev. *115*, 5891–5928.

184. Fang, S., and Hu, Y.H. (2021). Cyclo[18]carbon as an ultra-elastic molecular O-ring with unique mechanical properties. Carbon *171*, 96–103.

185. Baryshnikov, G.V., Valiev, R.R., Kuklin, A.V., Sundholm, D., and Ågren, H. (2019). Cyclo[18]carbon: insight into electronic structure, aromaticity, and surface coupling. J. Phys. Chem. Lett. *10*, 6701–6705.